10.1071/CH21314
Australian Journal of Chemistry

Supplementary Material

Synthesis of heteroleptic yttrium and dysprosium 1,2,4-tris (trimethylsilyl)cyclopentadienyl complexes

Sophie C. Corner[A], *Conrad A. P. Goodwin*[A], *Fabrizio Ortu*[A,B], *Peter Evans*[A], *Hongrui Zhang*[A], *Gemma K. Gransbury*[A], *George F. S. Whitehead*[A] and *David P. Mills*[A,*]

[A]Department of Chemistry, The University of Manchester, Oxford Road, Manchester M13 9PL, UK

[B]Present address: School of Chemistry, University of Leicester, University Road, Leicester LE1 7RH, UK

*Correspondence to: Email: david.mills@manchester.ac.uk

Synthesis of heteroleptic yttrium and dysprosium 1,2,4-tris(trimethylsilyl)cyclopentadienyl complexes

Sophie C. Corner,[1†] Conrad A. P. Goodwin,[1†] Fabrizio Ortu,[1‡] Peter Evans,[1] Hongrui Zhang,[1] Gemma K. Gransbury,[1] George F. S. Whitehead,[1] and David P. Mills*[1]

[1]Department of Chemistry, The University of Manchester, Oxford Road, Manchester, M13 9PL, U.K.

*david.mills@manchester.ac.uk.

[†]These authors contributed equally to the work.

[‡]Current address: School of Chemistry, University of Leicester, University Road, Leicester, LE1 7RH, U.K.

Contents

1. Synthetic procedure for $[NEt_3H][BPh_4]$

$[NEt_3H][BPh_4]$. In air, $NaBPh_4$ (25.000 g, 73.1 mmol) was added to a single-neck 1 L round bottomed flask. The solid was dissolved in deionised water (400 mL) at room temperature, and then cooled to 0 °C in an ice bath. With vigorous stirring, $Et_3N{\cdot}HCl$ (10.055 g, 73.1 mmol) was added in a single portion, which resulted in the rapid precipitation of a white solid and the vessel became very slightly warm. Stirring and manual agitation were continued for 1 hour, then the mixture was filtered through a medium porosity fritted funnel and the solids collected. The white solids were washed with deionised water (100 mL), followed by hot deionised water (2 × 200 mL at 70 °C), and finally with Et_2O (2 × 100 mL). The flowing white powder was then transferred to a Schlenk and dried *in vacuo* at room temperature for 12 hours to give anhydrous $[NEt_3H][BPh_4]$ as a white solid. Yield: 29.420 g, 96%. Recrystallization of a small portion of the solid from THF at 5 °C gave crystals of $[NEt_3H][BPh_4]{\cdot}THF$ as large colourless blocks.

Data for $[NEt_3H][BPh_4]$: υ_{max} (Nujol)/cm^{-1} 3132 (m, N-H stretch), 3054 (m, C-H stretch arom.), 2984 (m, C-H stretch aliph.), 1580 (w, C-C stretch arom.), 1474 (m) 1424 (m), 1385 (m), 1264 (w), 1161 (m), 1065 (m), 1030 (m), 1011 (m), 863 (w), 839 (m), 808 (w), 773 (w), 738 (s), 703 (s), 604 (s), 460 (m), 432 (w). δ_H (d_6-DMSO) 7.18 (br m, 8H, *m*-C*H*), 6.98 (t, $^3J_{HH}$ = 7.4 Hz, 8H, *o*-C*H*), 6.80 (t, $^3J_{HH}$ = 7.1 Hz, 4H, *p*-C*H*), 3.05 (q, $^3J_{HH}$ = 7.3 Hz, 6H, $N(CH_2CH_3)_3$), 1.15 (t, $^3J_{HH}$ = 7.3 Hz, 9H, $N(CH_2CH_3)_3$), N*H* not observed. δ_B (d_6-DMSO) –6.69 (*B*Ph_4). δ_C (d_6-DMSO) 163.58 (q, $^1J_{BH}$ = 49.5 Hz, *ipso*-C), 135.75 (*m*-*C*H), 125.60 (q, $^4J_{BH}$ = 2.9 Hz, *m*-*C*H), 121.85 (*p*-*C*H), 46.08 ($N(CH_2CH_3)_3$), 8.85 ($N(CH_2CH_3)_3$). Anal. Calc. for $C_{30}H_{36}BN$: C 85.50, H 8.61, N 3.32. Found: C 84.78, H 8.57, N 3.32%.

2. NMR spectroscopic data for 1-6, [NEt$_3$H][BPh$_4$] and reaction mixtures

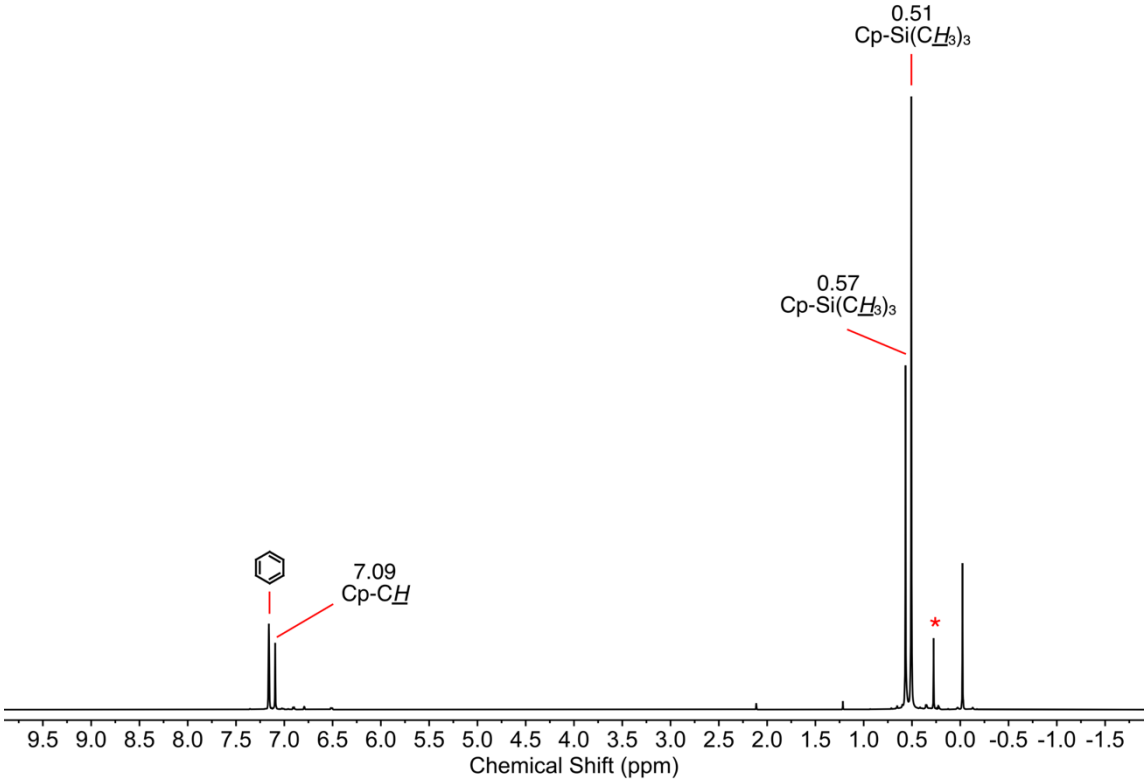

Figure S1. ^{1}H NMR spectrum of **1-Y** in d_6-benzene. * denotes Si grease impurity.

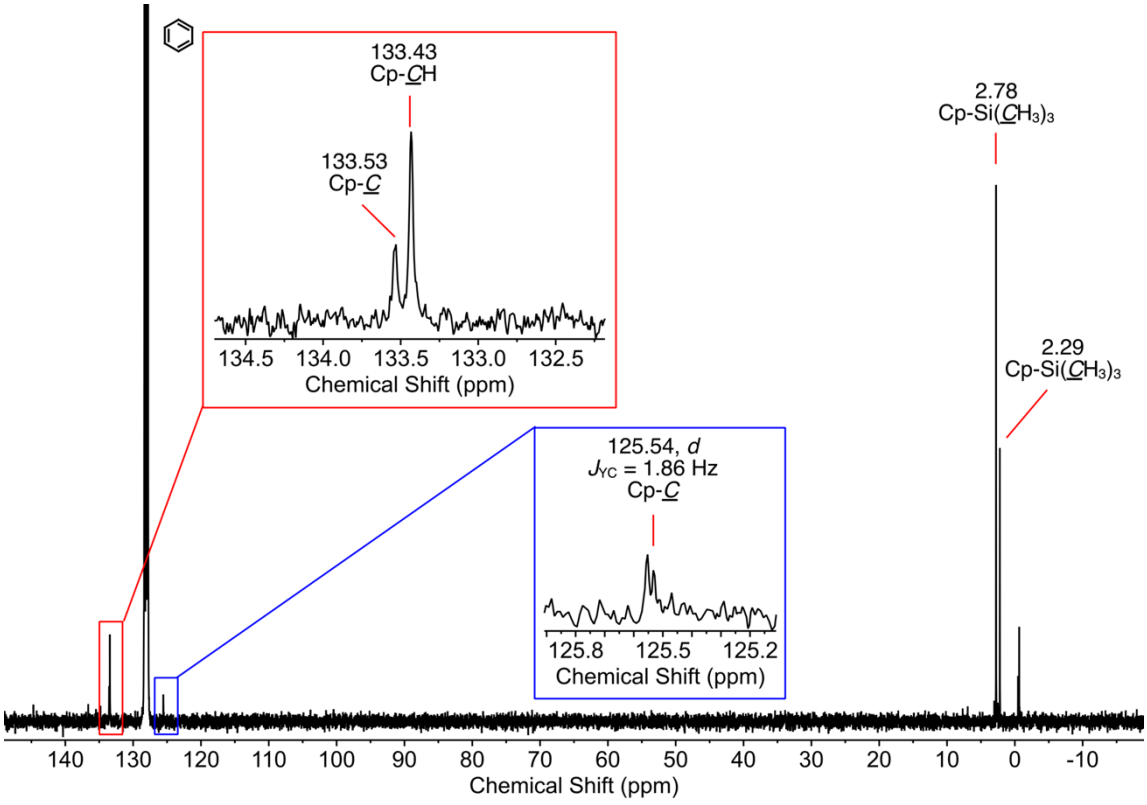

Figure S2. ^{13}C{^{1}H} NMR spectrum of **1-Y** in d_6-benzene.

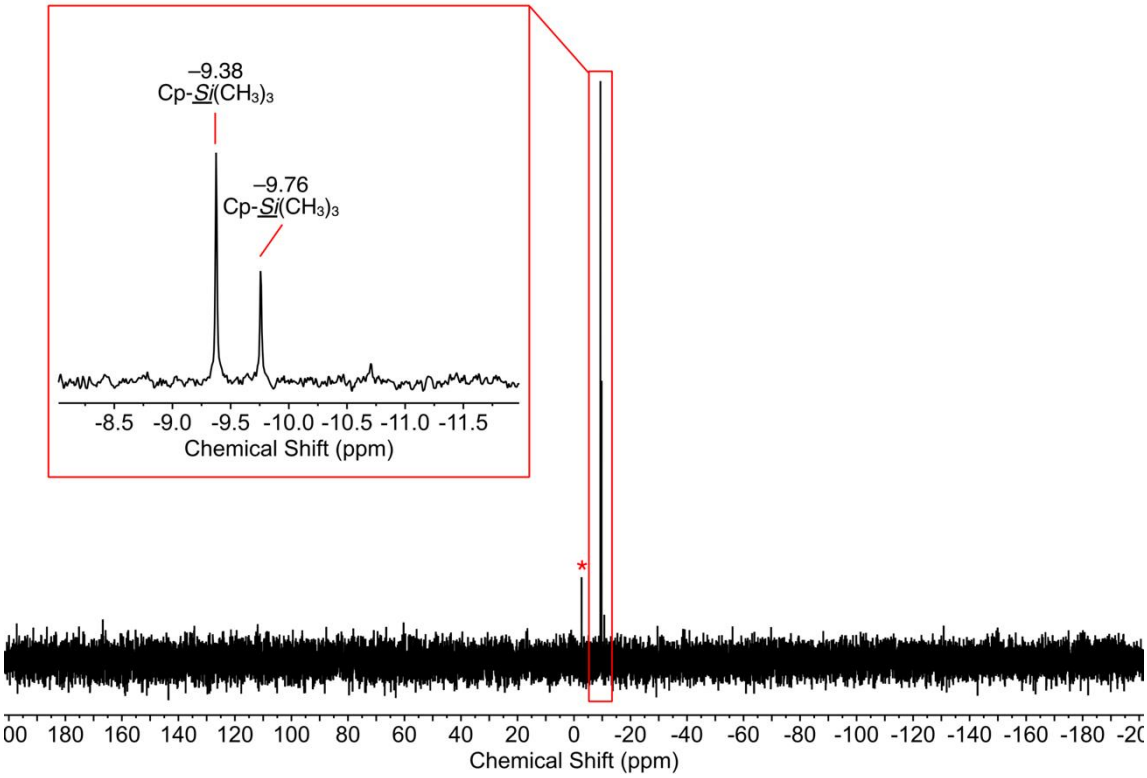

Figure S3. $^{29}Si\{^{1}H\}$ NMR spectrum of **1-Y** in d_6-benzene. * denotes Si-grease impurity.

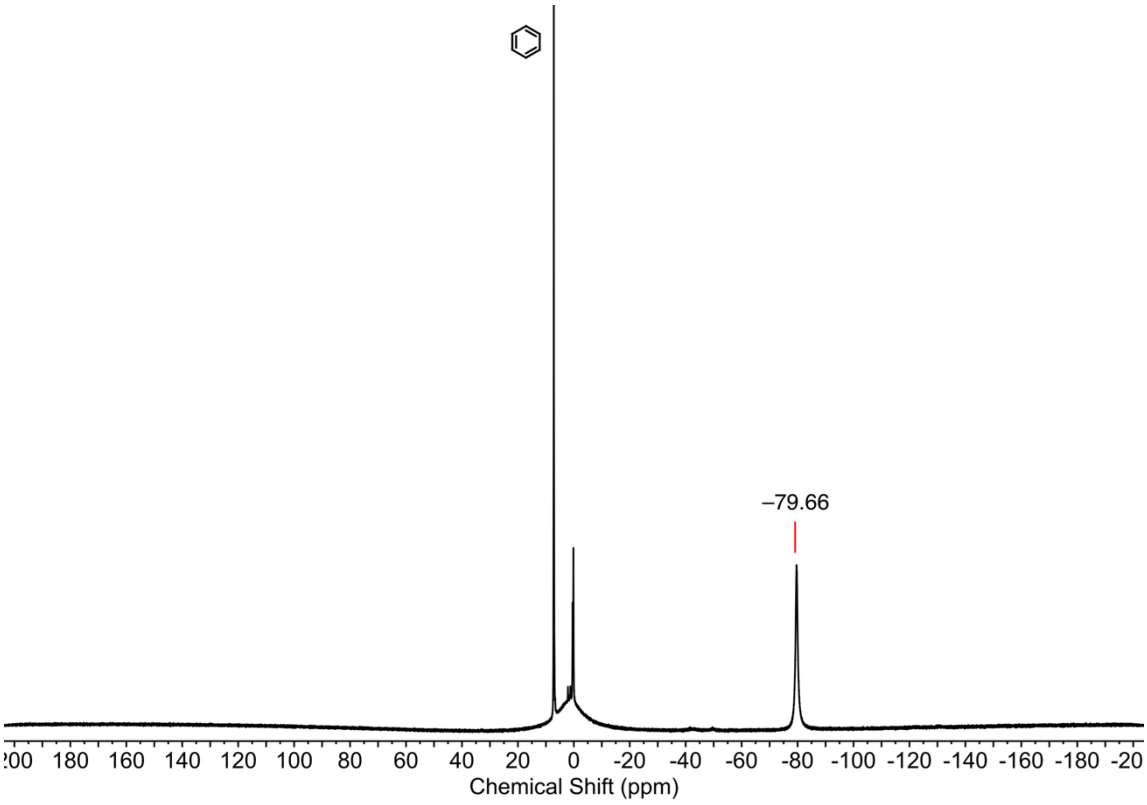

Figure S4. ^{1}H NMR spectrum of **1-Dy** in d_6-benzene.

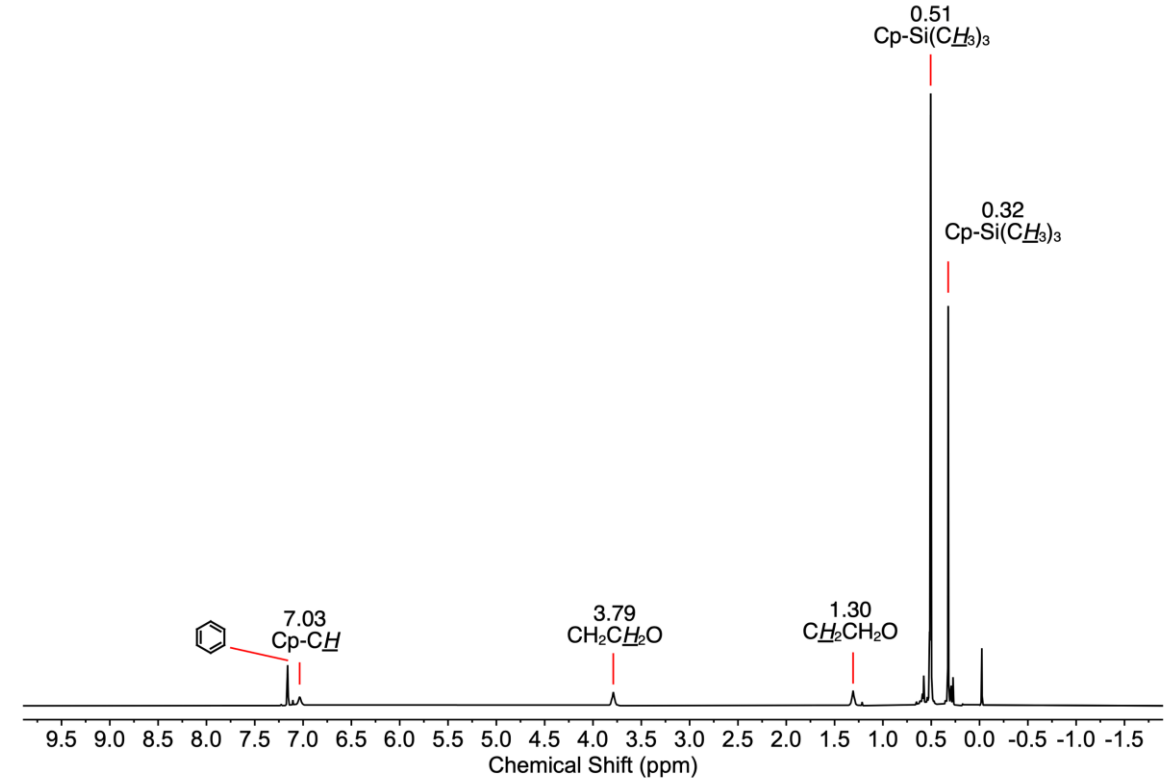

Figure S5. ^{1}H NMR spectrum of **2-Y** in d_6-benzene.

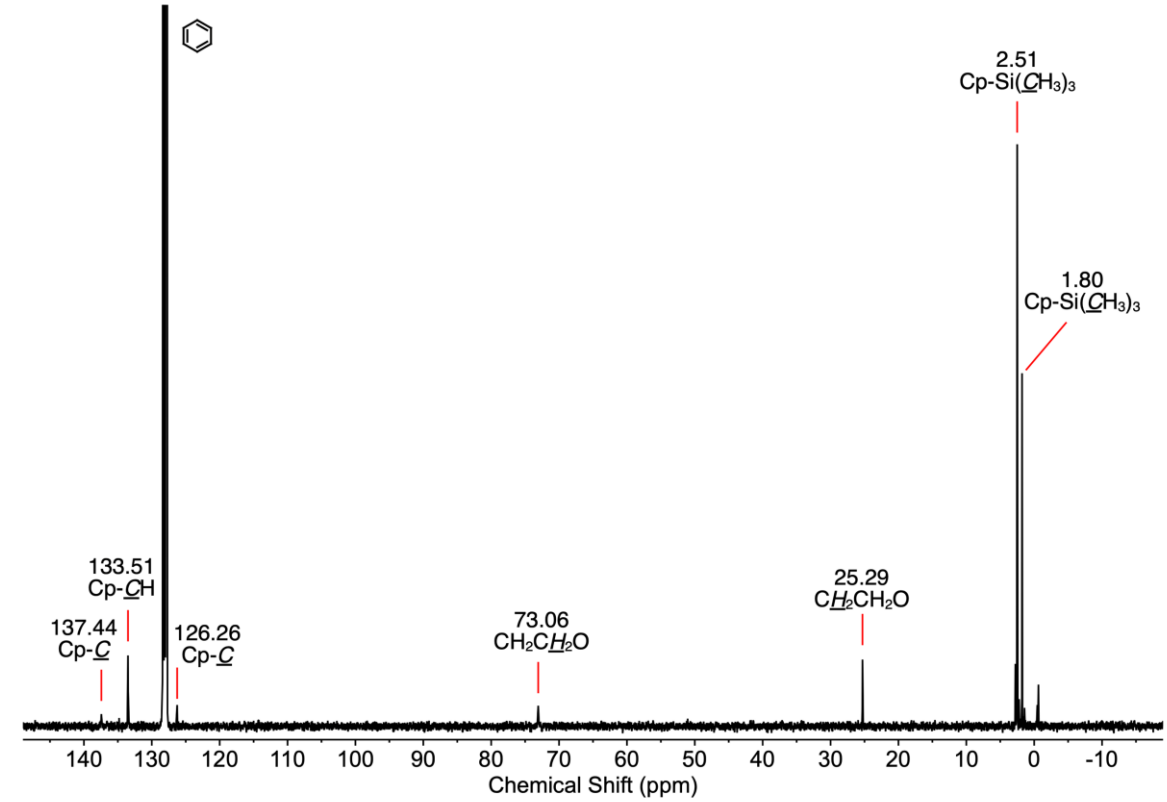

Figure S6. ^{13}C{^{1}H} NMR spectrum of **2-Y** in d_6-benzene.

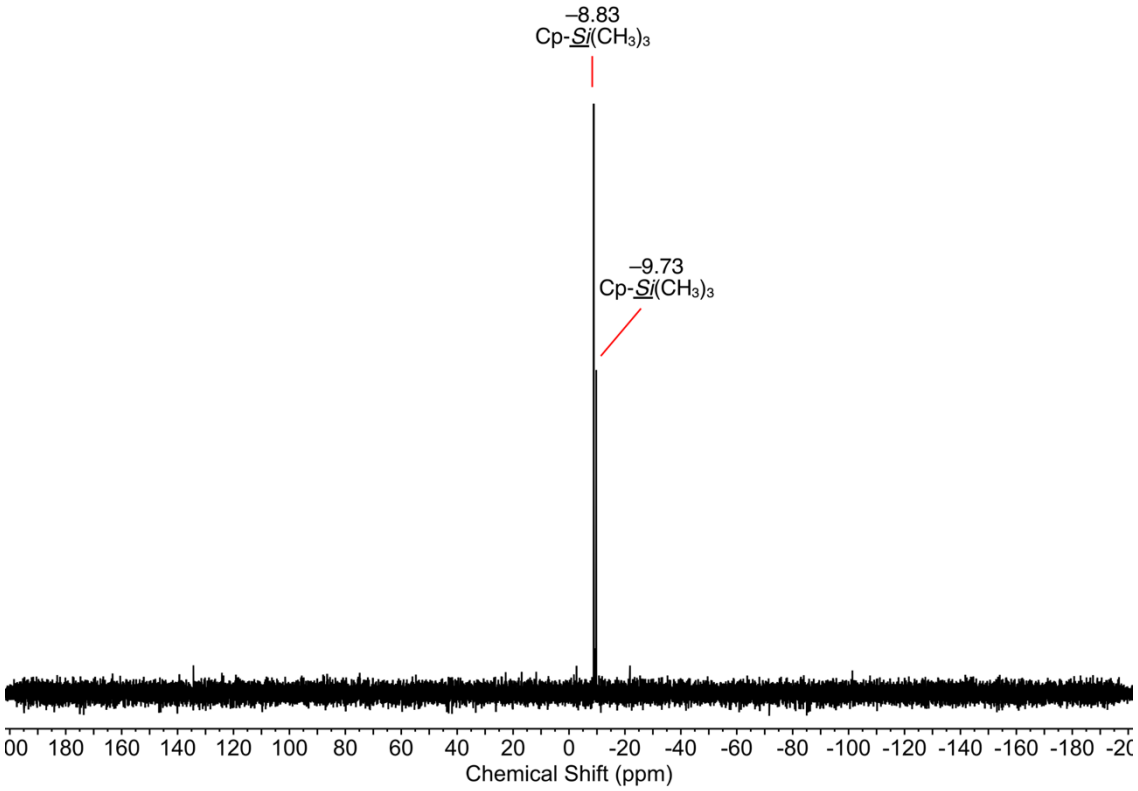

Figure S7. $^{29}Si\{^{1}H\}$ NMR spectrum of **2-Y** in d_6-benzene.

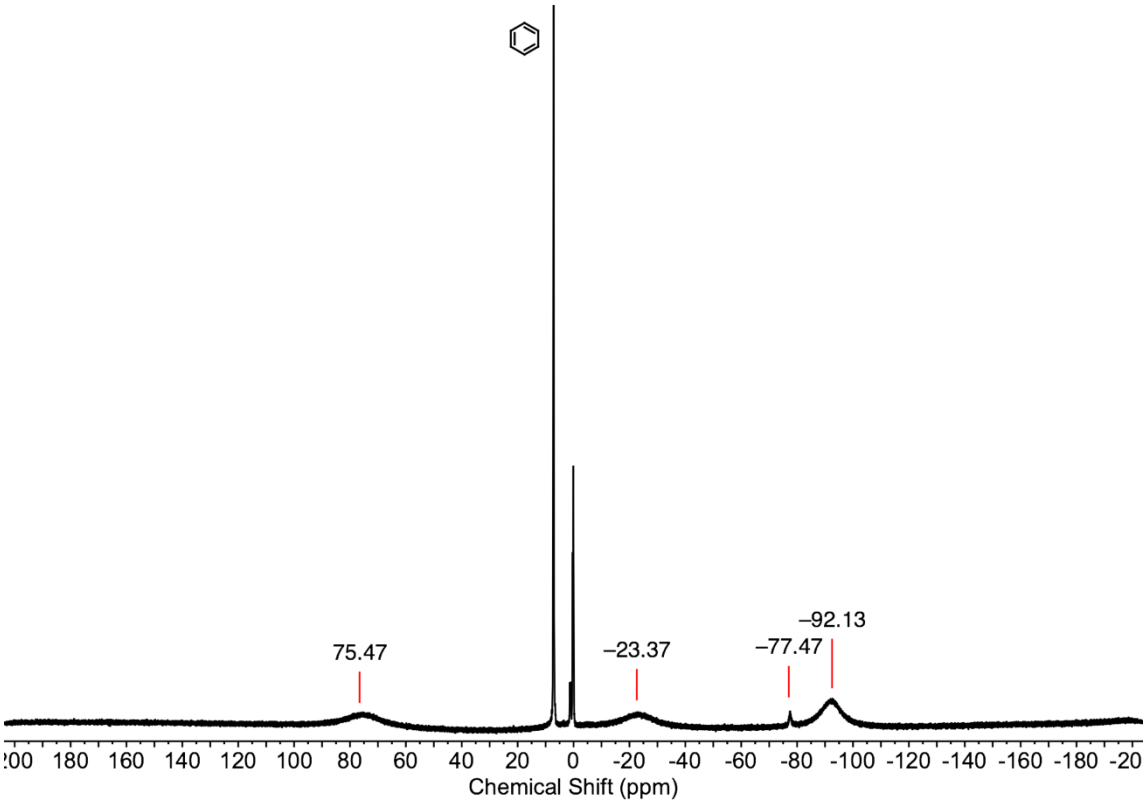

Figure S8. ^{1}H NMR spectrum of **2-Dy** in d_6-benzene.

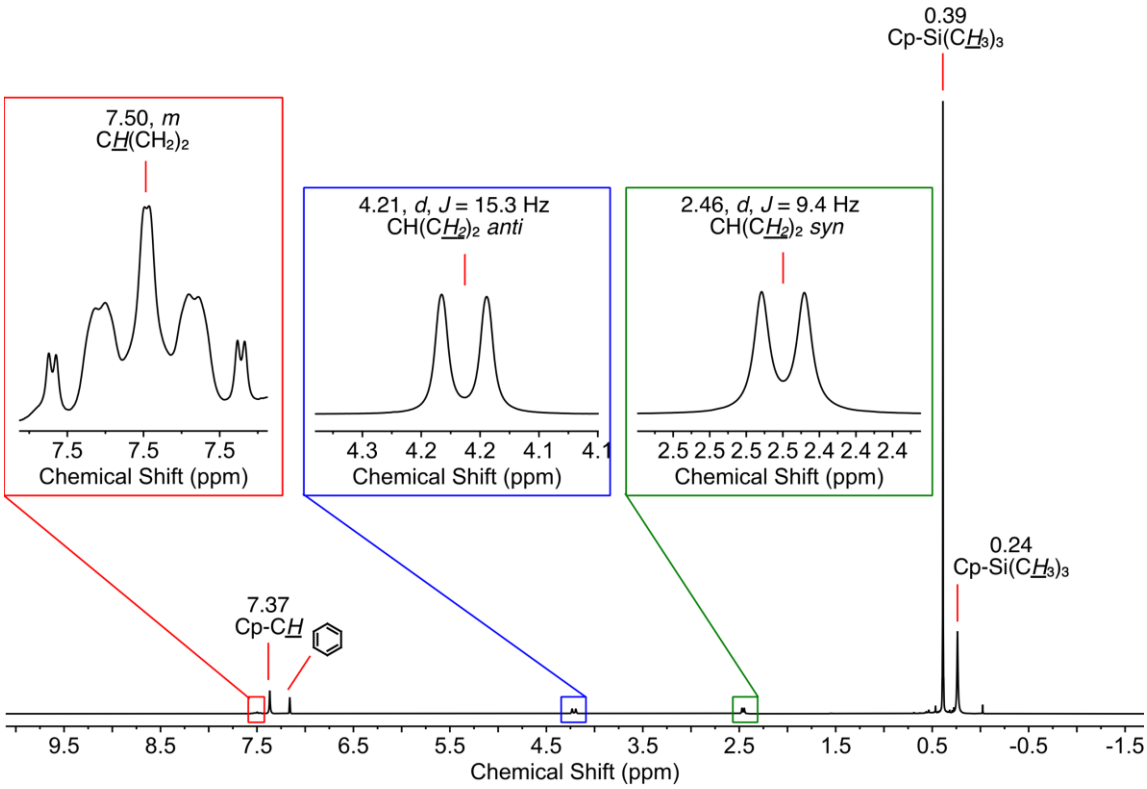

Figure S9. ^{1}H NMR spectrum of **3-Y** in d_6-benzene.

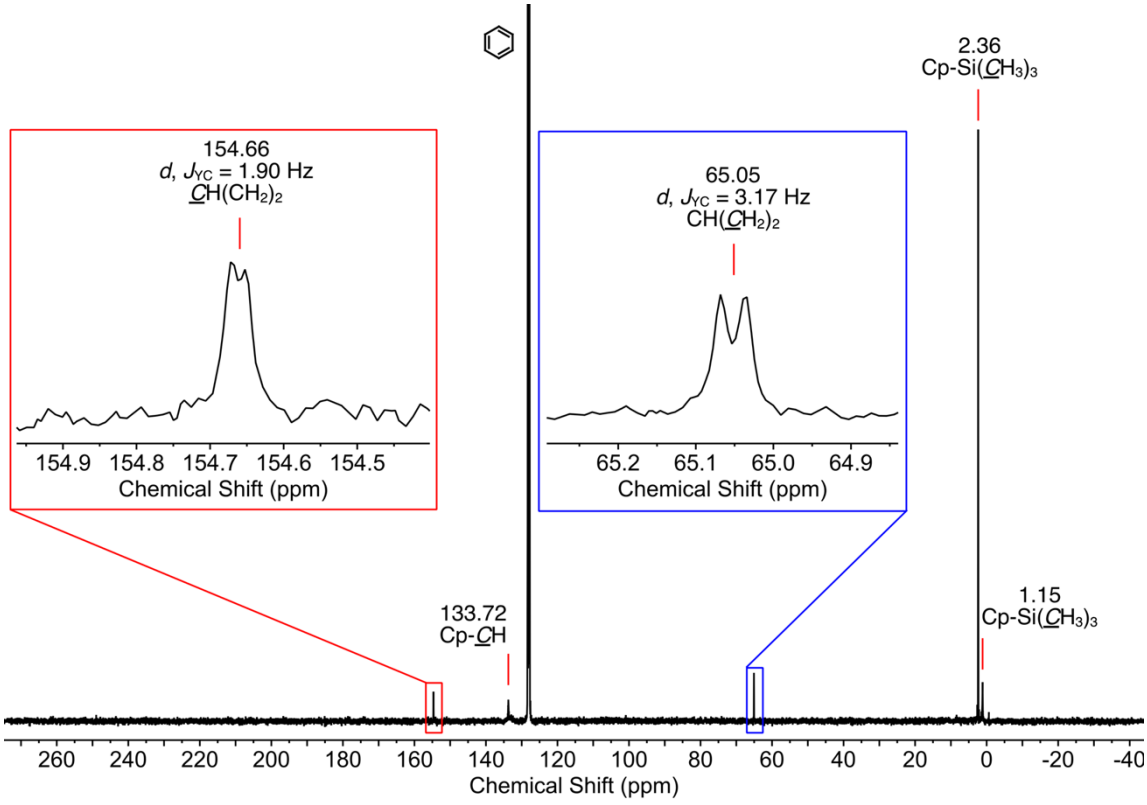

Figure S10. ^{13}C{^{1}H} NMR spectrum of **3-Y** in d_6-benzene.

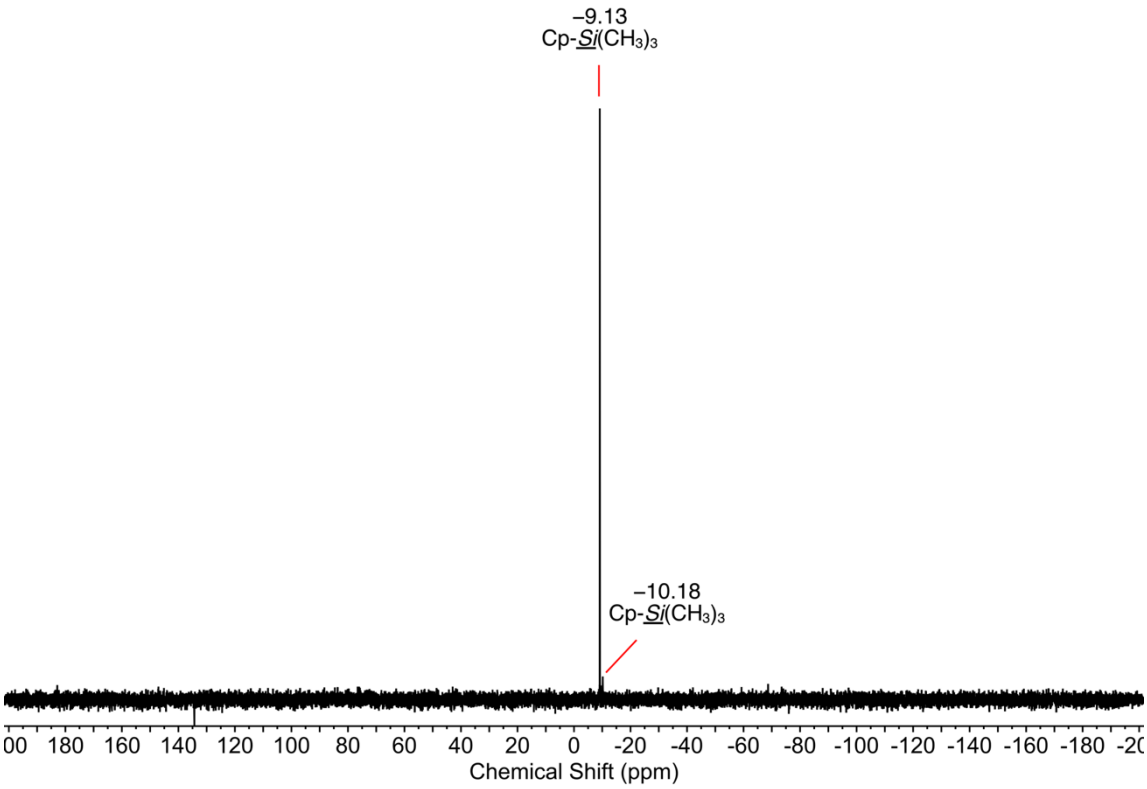

Figure S11. ^{29}Si INEPT NMR spectrum of **3-Y** in d_6-benzene.

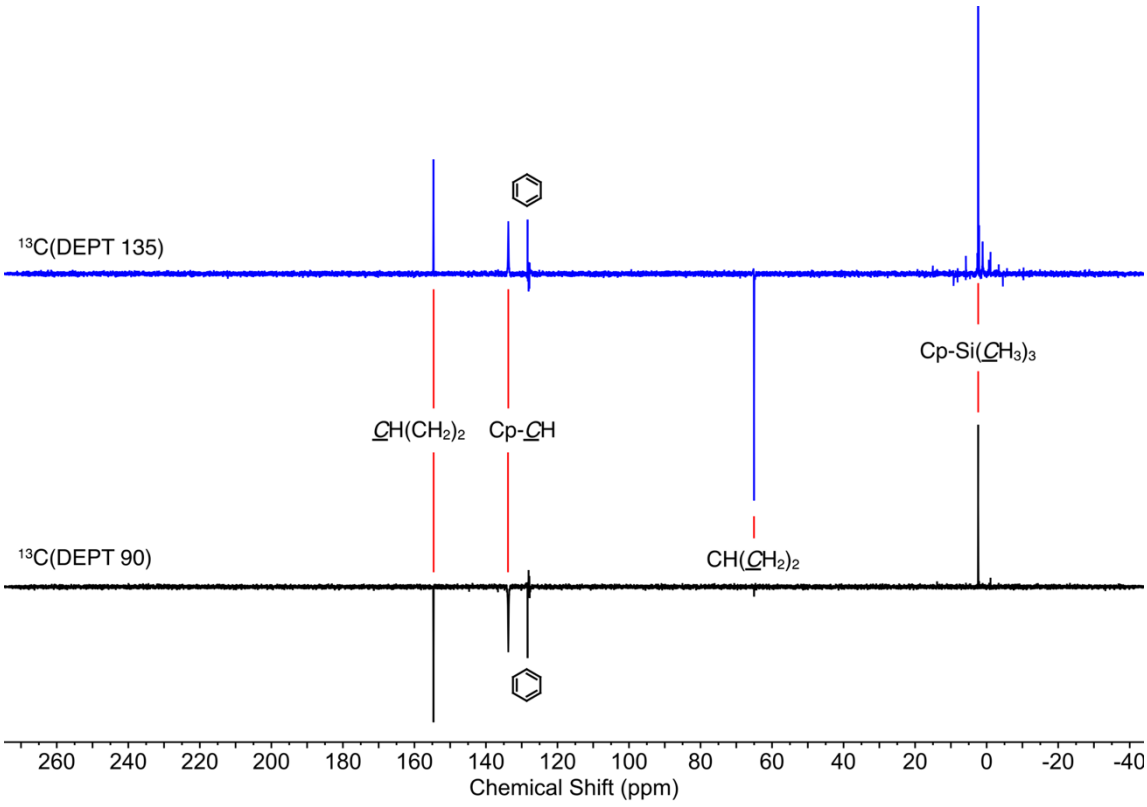

Figure S12. Combined ^{13}C DEPT 90 and DEPT 135 NMR spectra of **3-Y** in d_6-benzene.

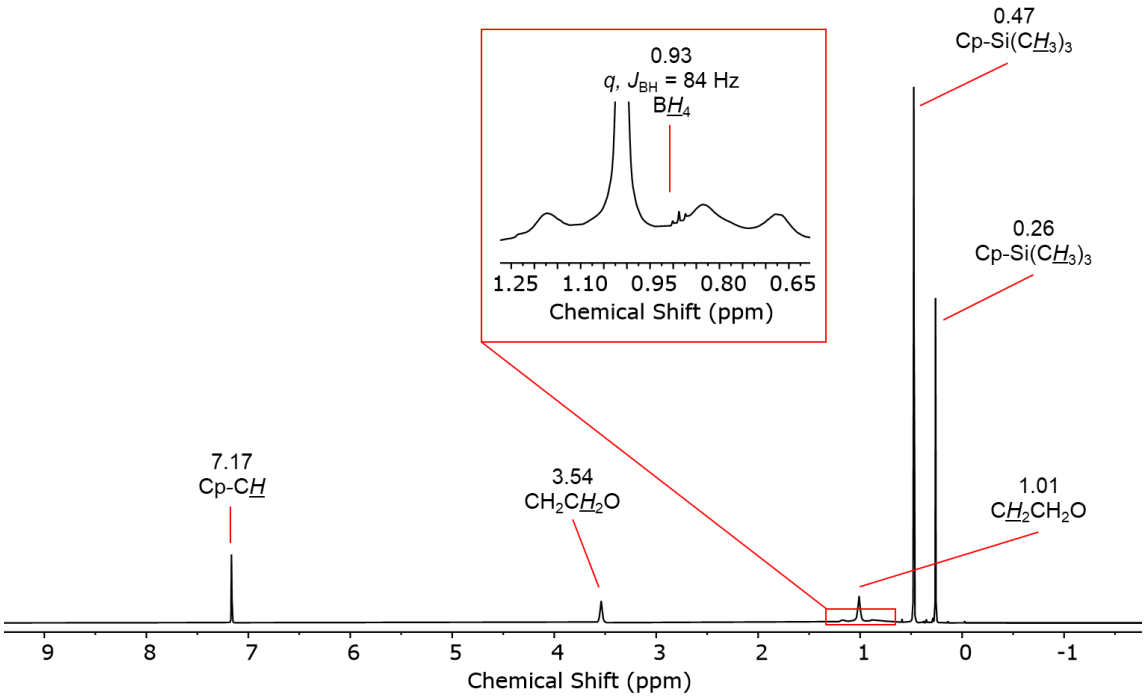

Figure S13. ^{1}H NMR spectrum of **4-Y** in d_6-benzene.

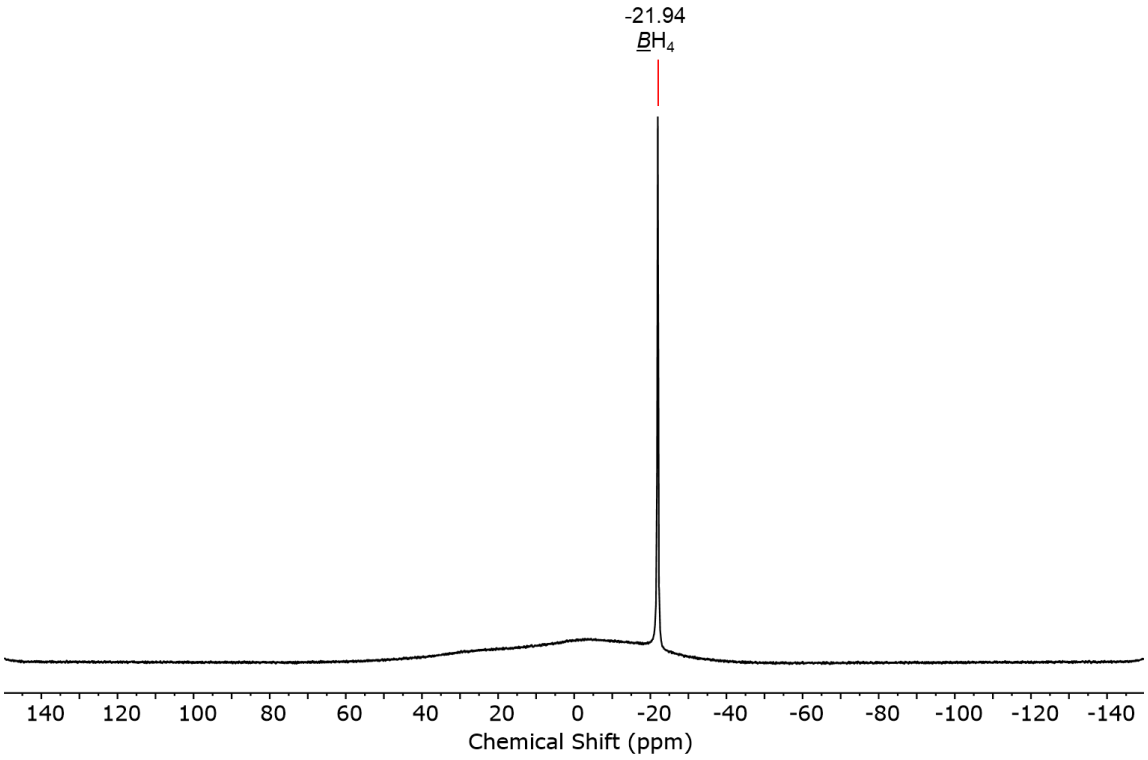

Figure S14. ^{11}B{^{1}H} NMR spectrum of **4-Y** in d_6-benzene.

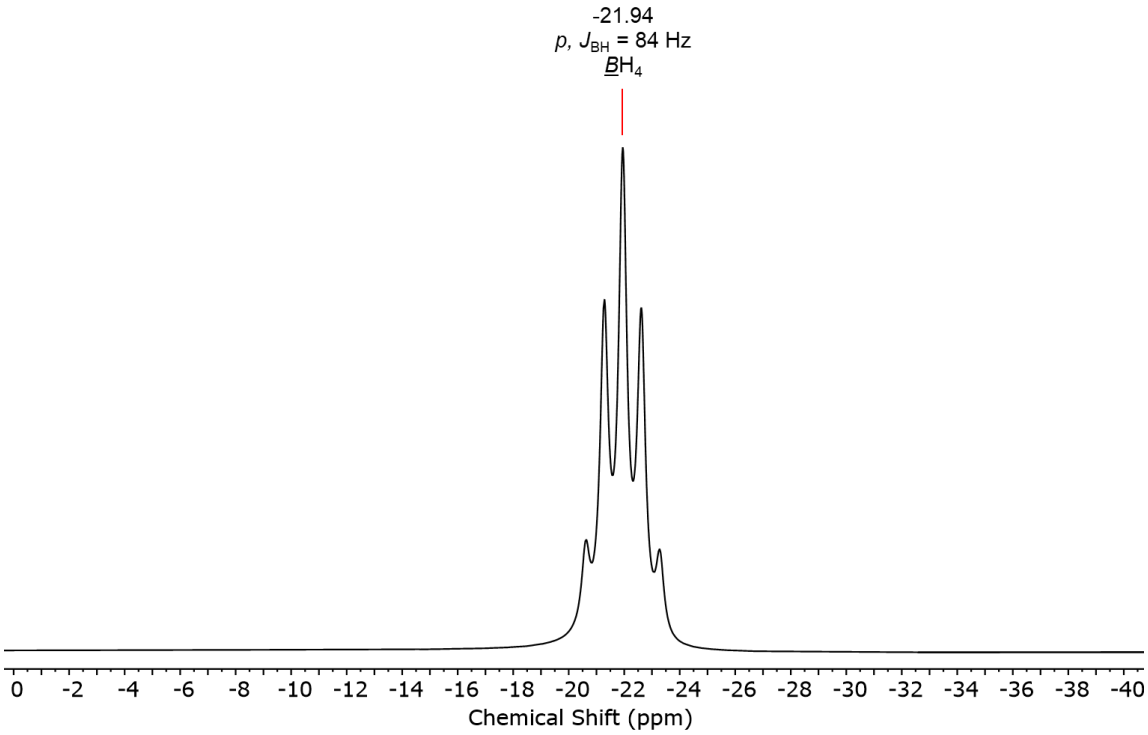

Figure S15. ^{11}B NMR spectrum of **4-Y** in d_6-benzene.

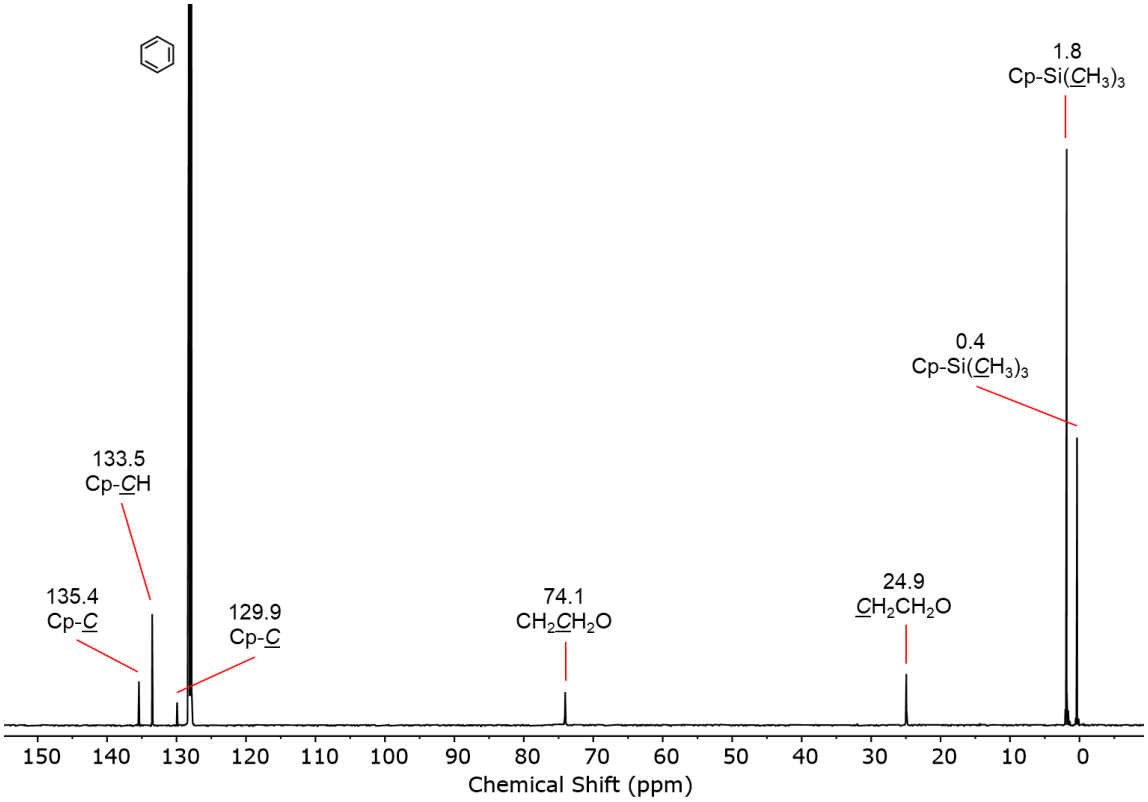

Figure S16. ^{13}C{^{1}H} NMR spectrum of **4-Y** in d_6-benzene.

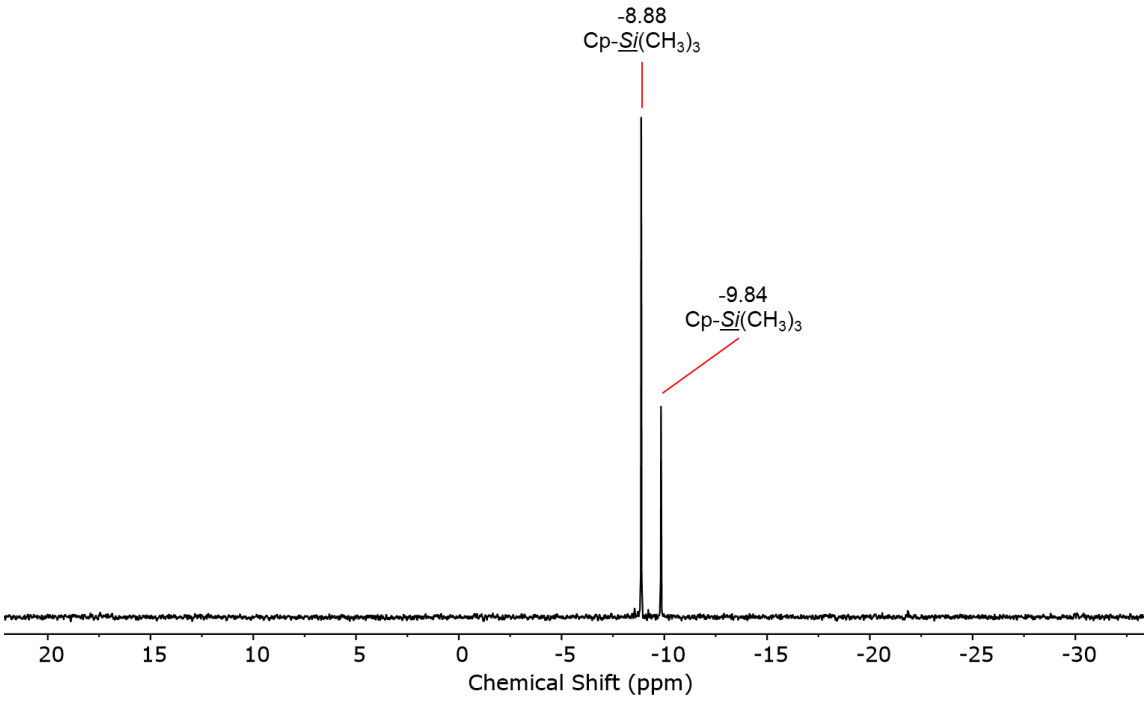

Figure S17. $^{29}Si\{^{1}H\}$ NMR spectrum of **4-Y** in d_6-benzene.

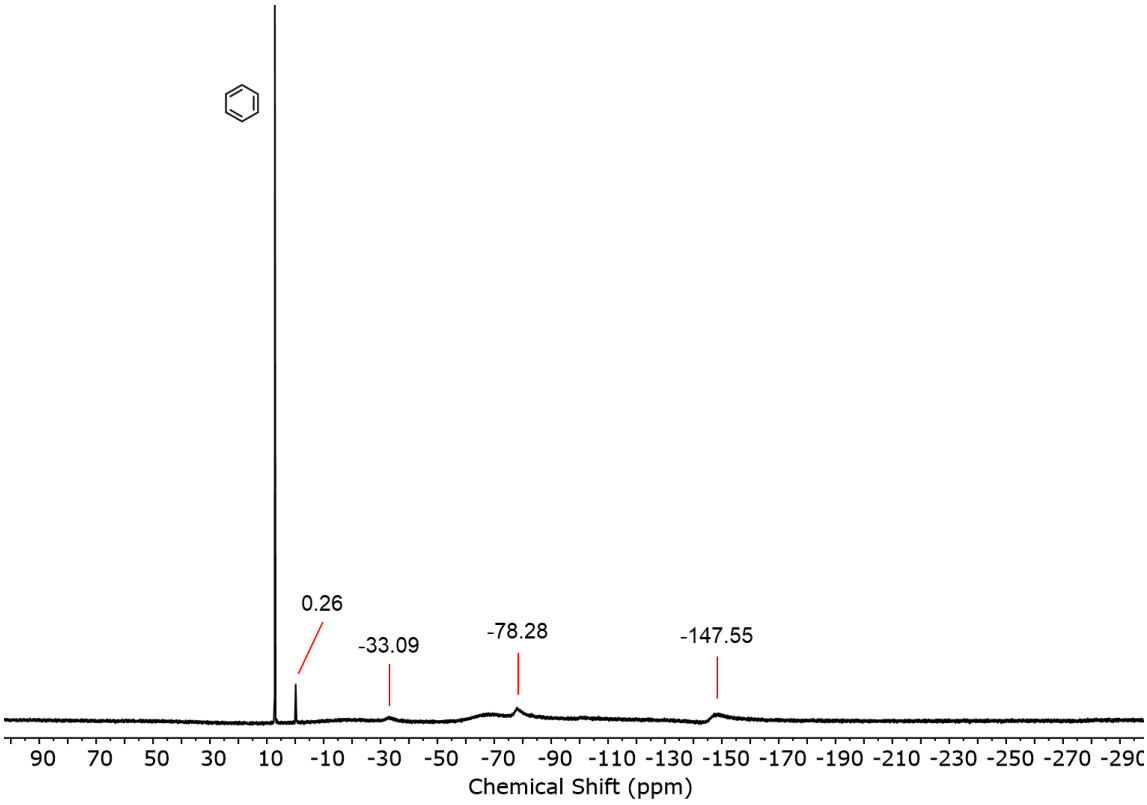

Figure S18. ^{1}H NMR spectrum of **5-Dy** in d_6-benzene.

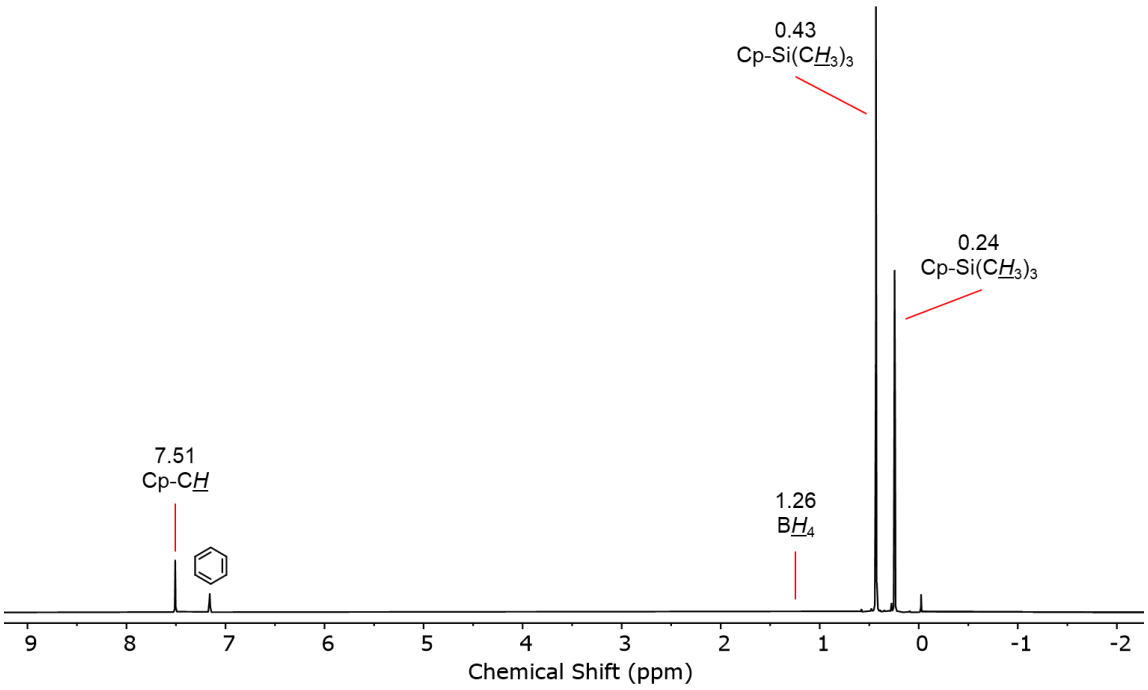

Figure S19. ^{1}H NMR spectrum of **6-Y** in d_6-benzene.

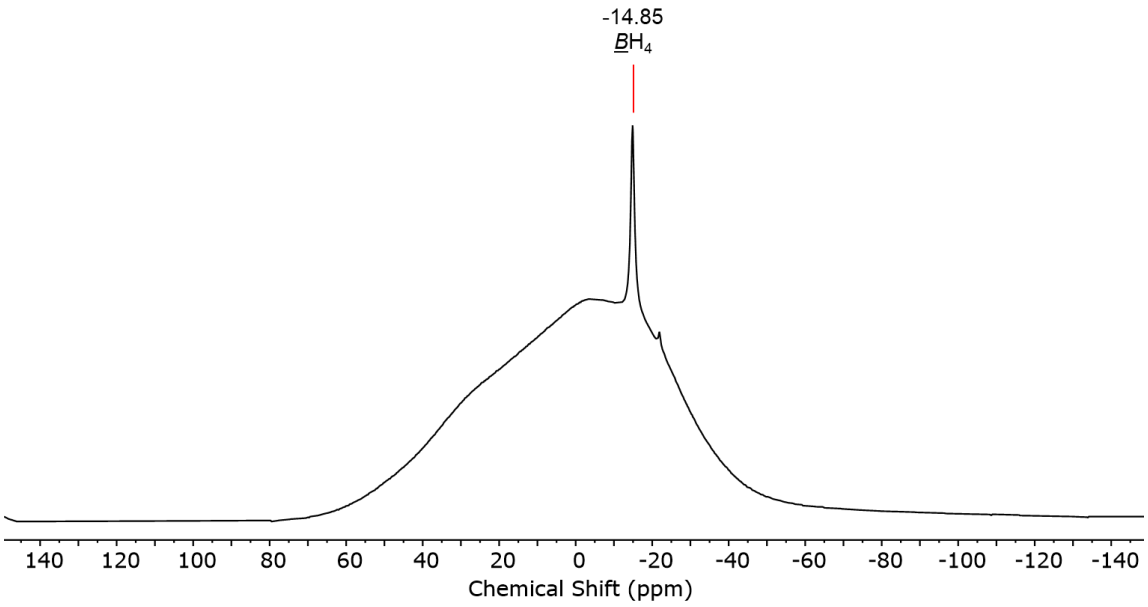

Figure S20. ^{11}B{^{1}H} NMR spectrum of **6-Y** in d_6-benzene.

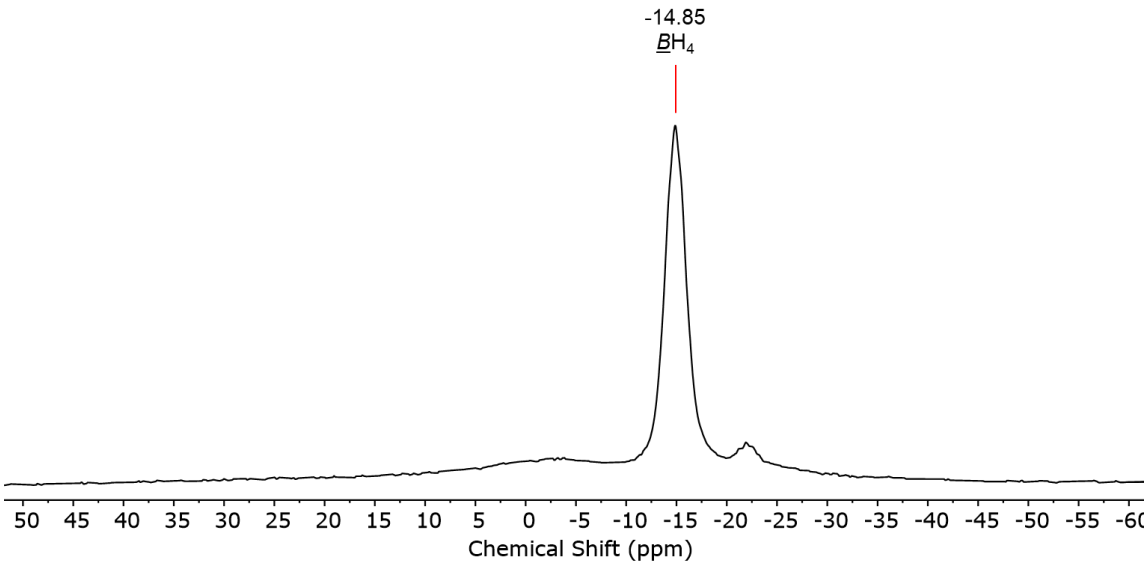

Figure S21. ^{11}B NMR spectrum of **6-Y** in d_6-benzene.

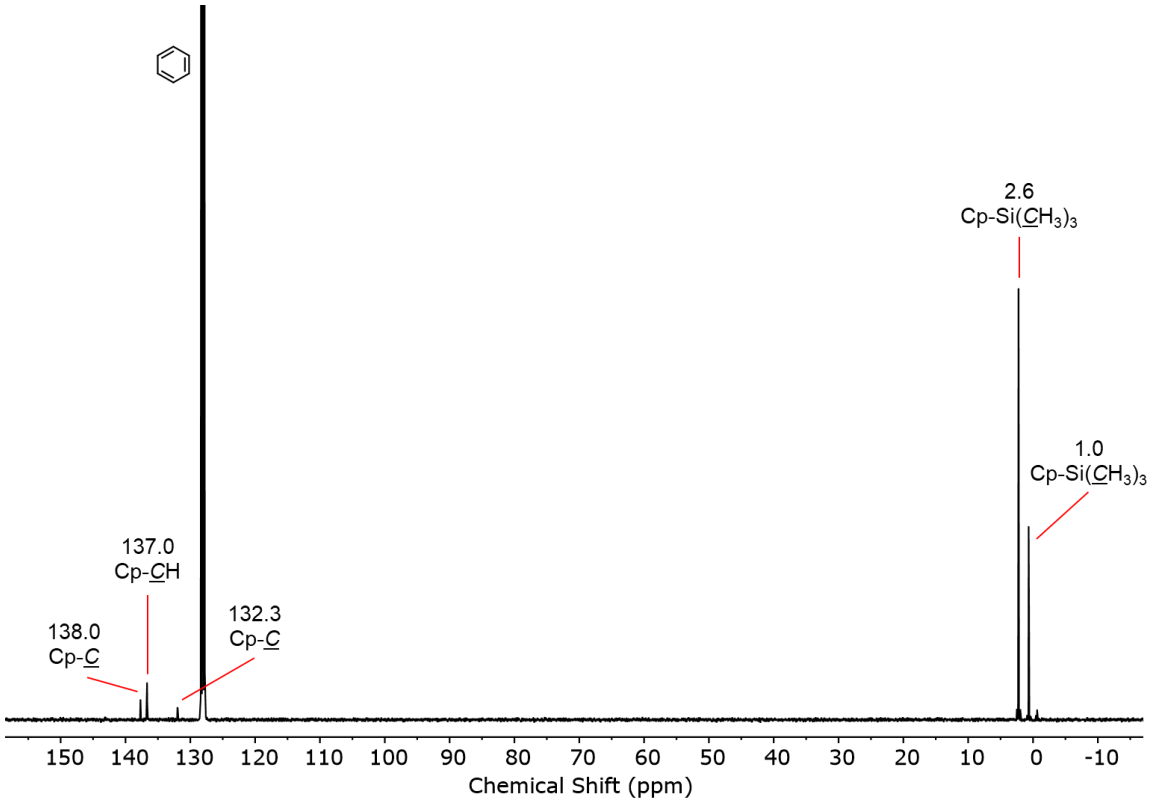

Figure S22. ^{13}C{^{1}H} NMR spectrum of **6-Y** in d_6-benzene.

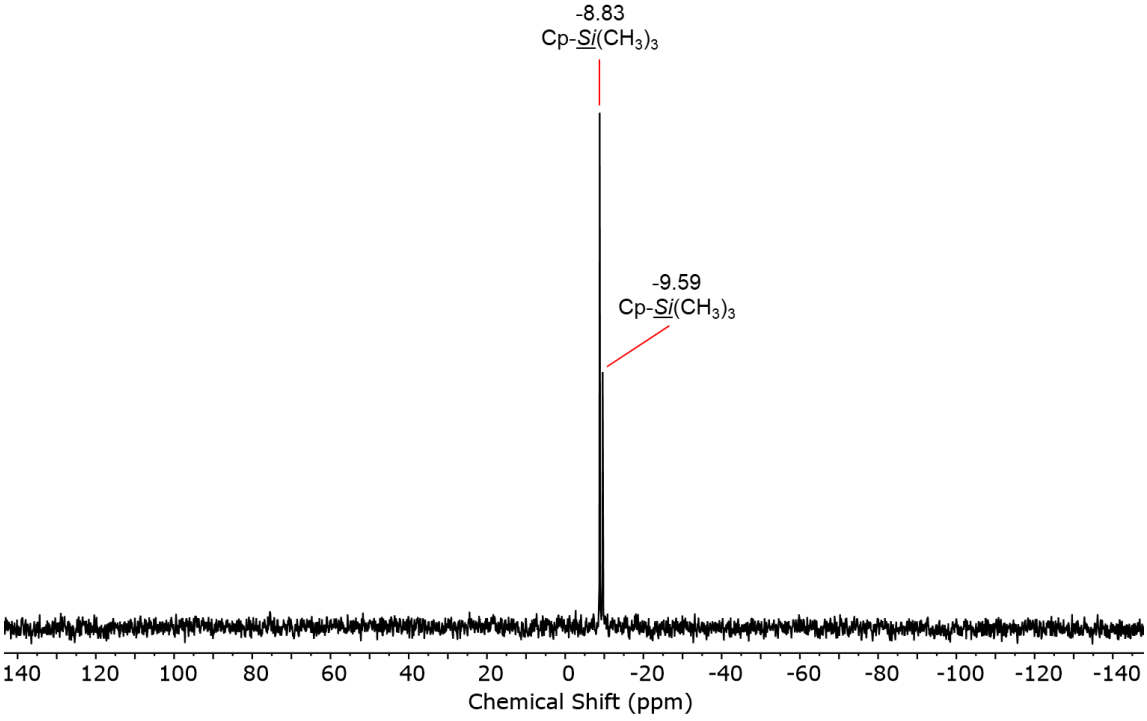

Figure S23. $^{29}Si\{^{1}H\}$ NMR spectrum of **6-Y** in d_6-benzene.

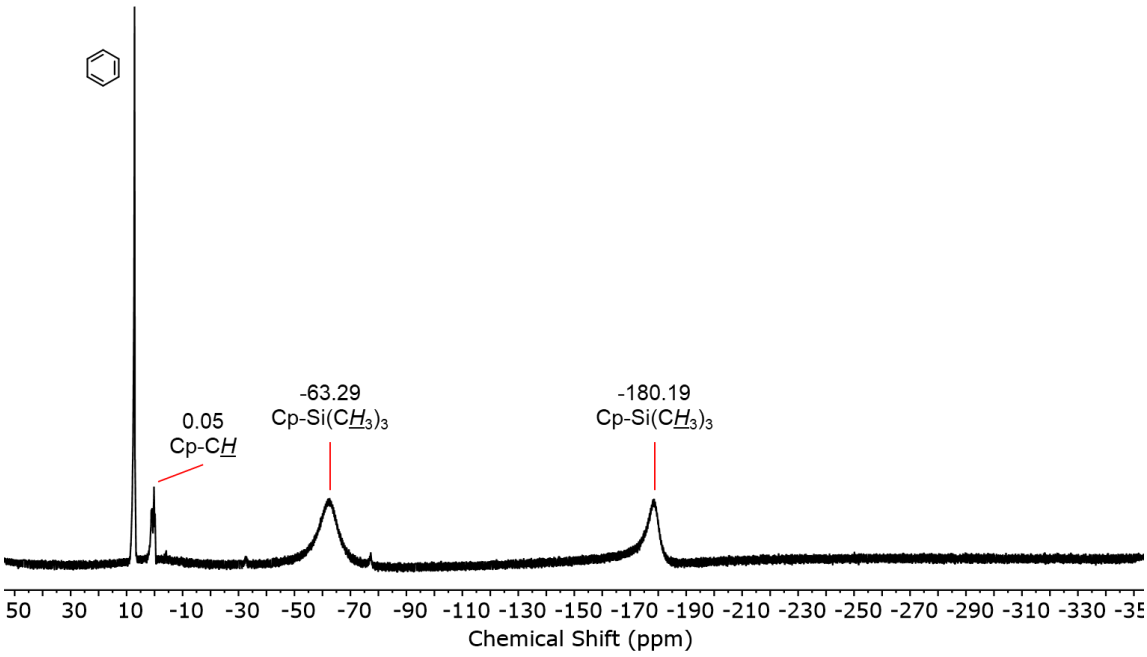

Figure S24. ^{1}H NMR spectrum of **6-Dy** in d_6-benzene.

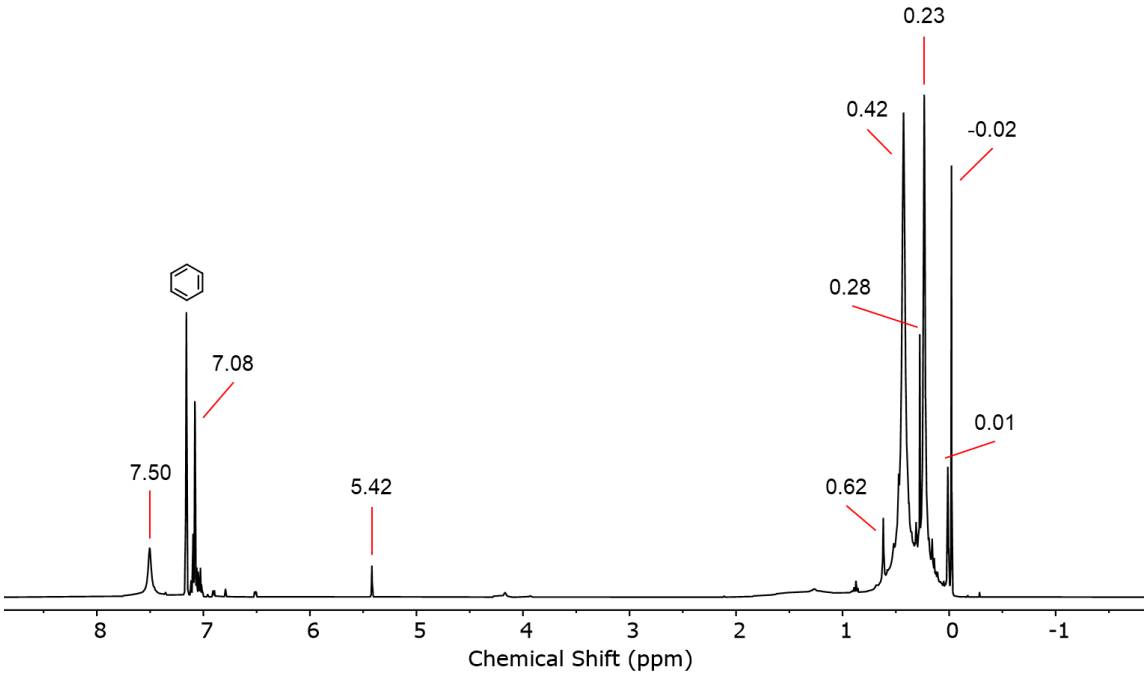

Figure S25. ^{1}H NMR spectrum of the reaction mixture between **6-Y** and $[CPh_3][B(C_6F_5)_4]$ in d_6-benzene.

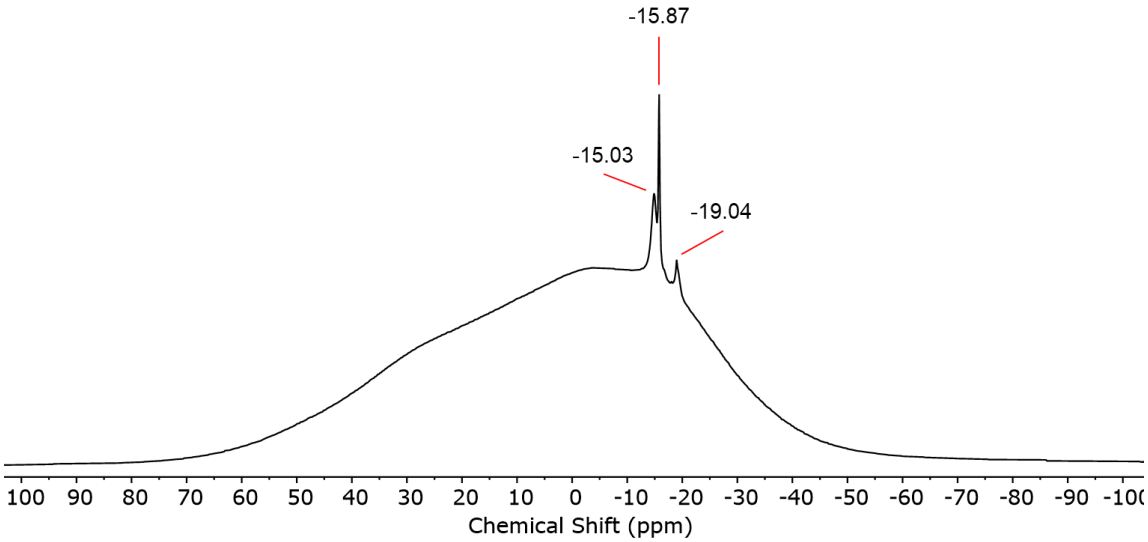

Figure S26. ^{11}B{^{1}H} NMR spectrum of the reaction mixture between **6-Y** and $[CPh_3][B(C_6F_5)_4]$ in d_6-benzene.

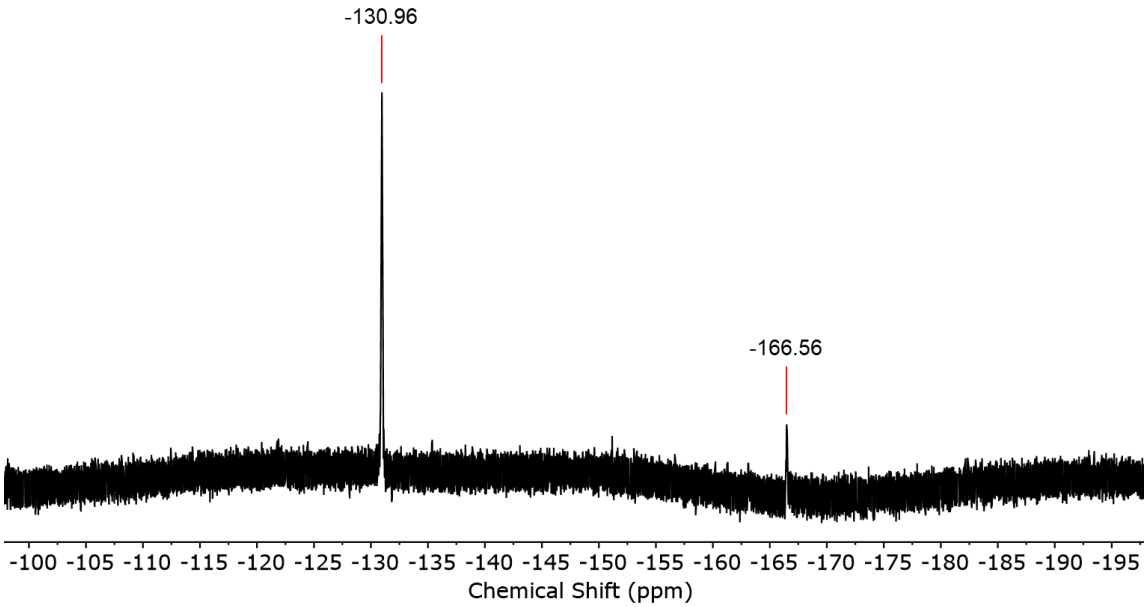

Figure S27. ^{19}F NMR spectrum of the reaction mixture between **6-Y** and $[CPh_3][B(C_6F_5)_4]$ in d_6-benzene.

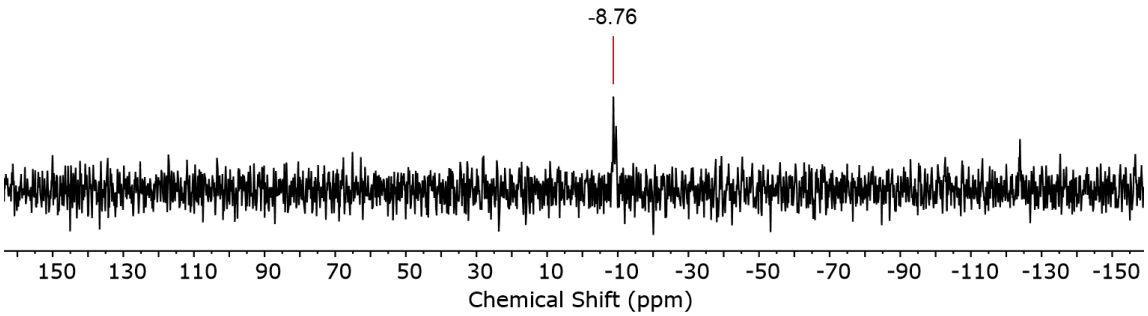

Figure S28. $^{29}Si\{^1H\}$ NMR spectrum of the reaction mixture between **6-Y** and $[CPh_3][B(C_6F_5)_4]$ in d_6-benzene.

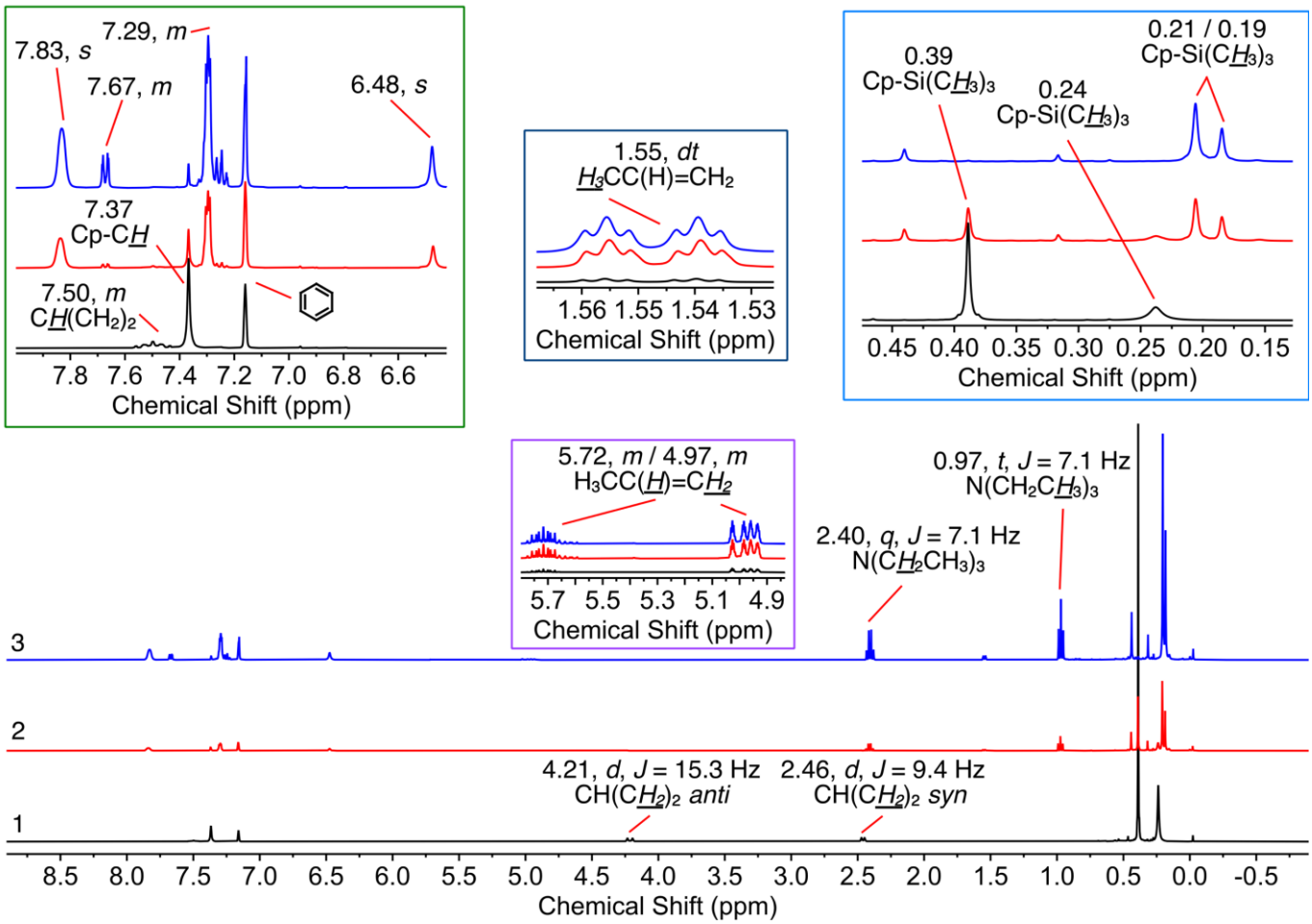

Figure S29. ^{1}H NMR spectra (collected *in situ*) of the reaction mixture between **3-Y** and [NEt_3H][BPh_4] in d_6-benzene. Spectrum 1 (bottom) corresponds to pure **3-Y** (as in Figure S9 above); Spectrum 2 (middle) is the reaction after 5 days at room temperature; Spectrum 3 (top) is the reaction mixture after 7 days at room temperature, followed by 2 hours at 80 °C. There is no time point for 7 days at room temperature without the heating – it was decided that the progress after 5 days suggested that further time at room temperature was unlikely to have driven the reaction to completion. Note in Spectrum 2 and 3 the presence of propene and NEt_3 in solution, along with the disappearance of peaks associated with **3-Y**.

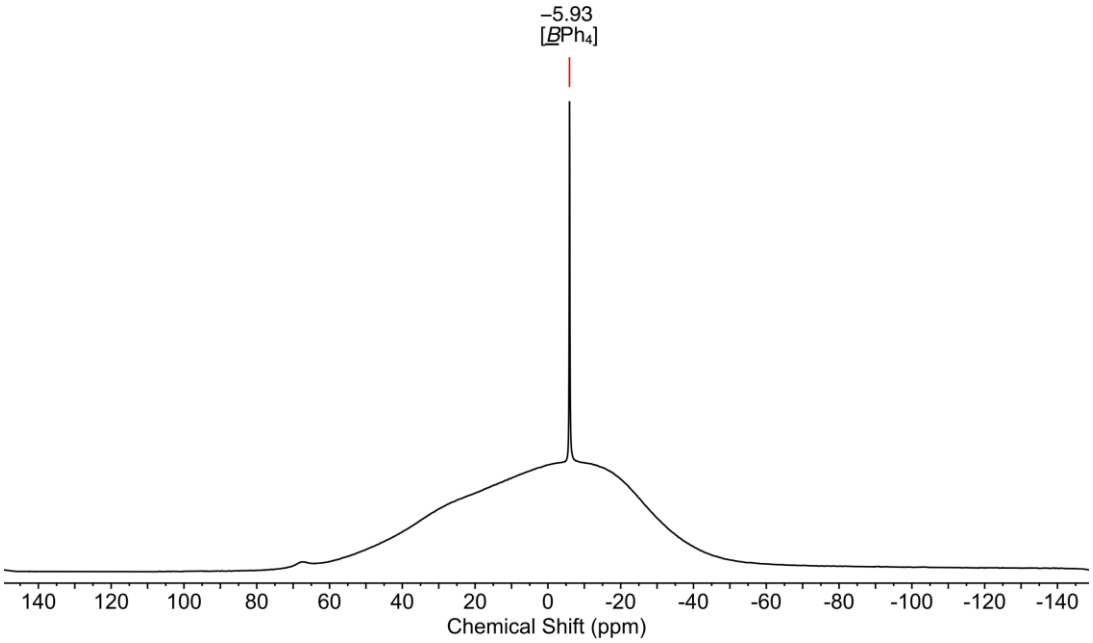

Figure S30. $^{11}B\{^{1}H\}$ NMR spectrum (collected *in situ*) of the reaction mixture between **3-Y** and $[NEt_3H][BPh_4]$ in d_6-benzene after 7 days at room temperature, followed by 2 hours at 80 °C. Note only a single major peak is observed; the resonance for BPh_3 would be expected around 68 ppm in d_6-benzene[1] and there is a small feature here.

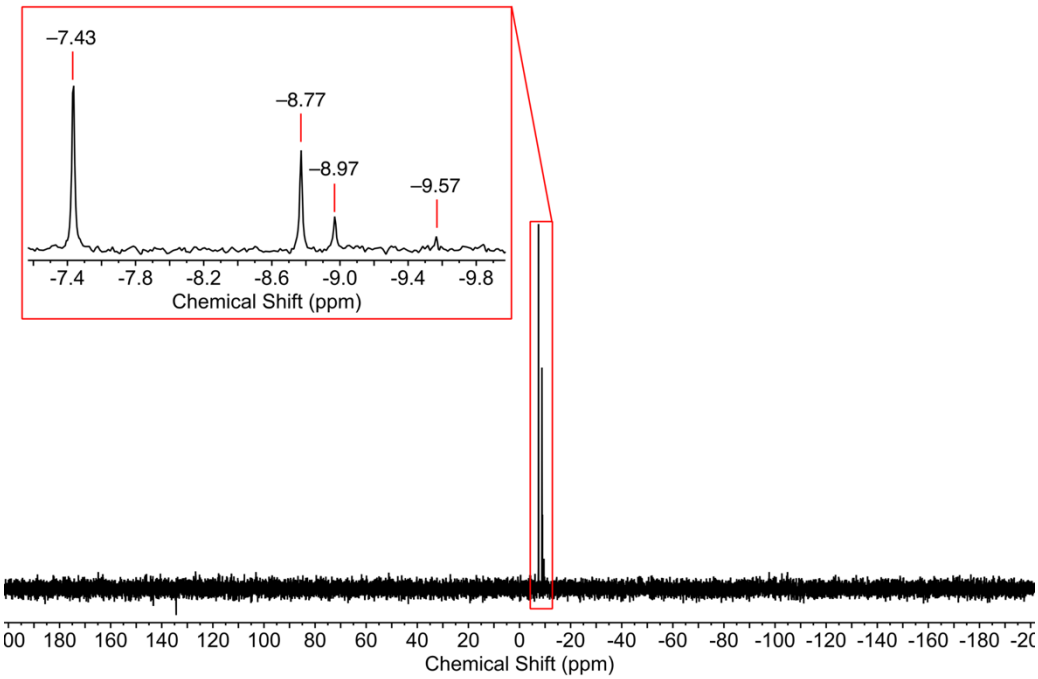

Figure S31. ^{29}Si INEPT NMR spectrum (collected *in situ*) of the reaction mixture between **3-Y** and $[NEt_3H][BPh_4]$ in d_6-benzene after 7 days at room temperature, followed by 2 hours at 80 °C.

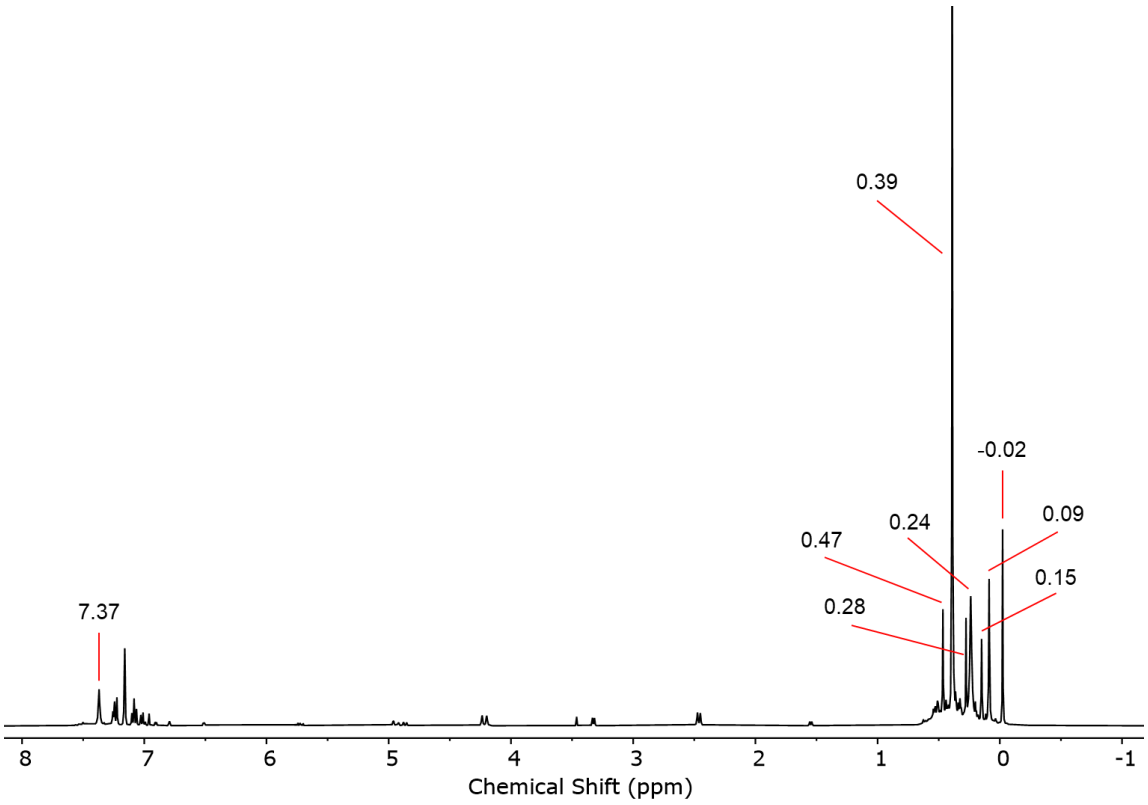

Figure S32. ^{1}H NMR spectrum of the reaction mixture between **3-Y** and [CPh$_3$][B(C$_6$F$_5$)$_4$] in d_6-benzene.

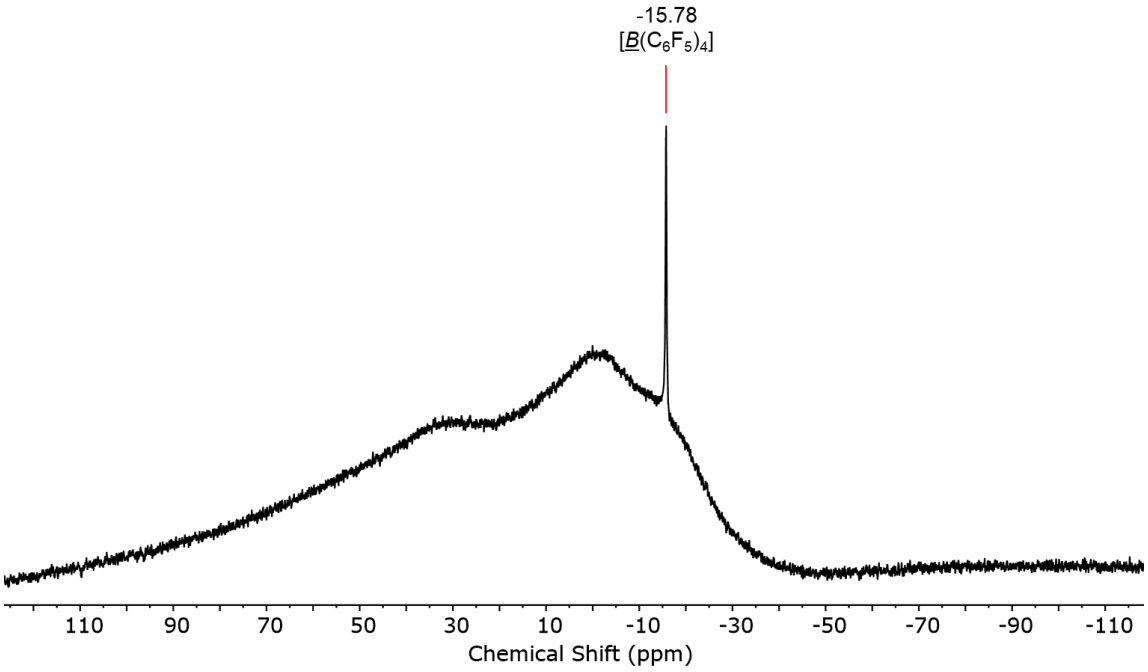

Figure S33. ^{11}B{^{1}H} NMR spectrum of the reaction mixture between **3-Y** and [CPh$_3$][B(C$_6$F$_5$)$_4$] in d_6-benzene.

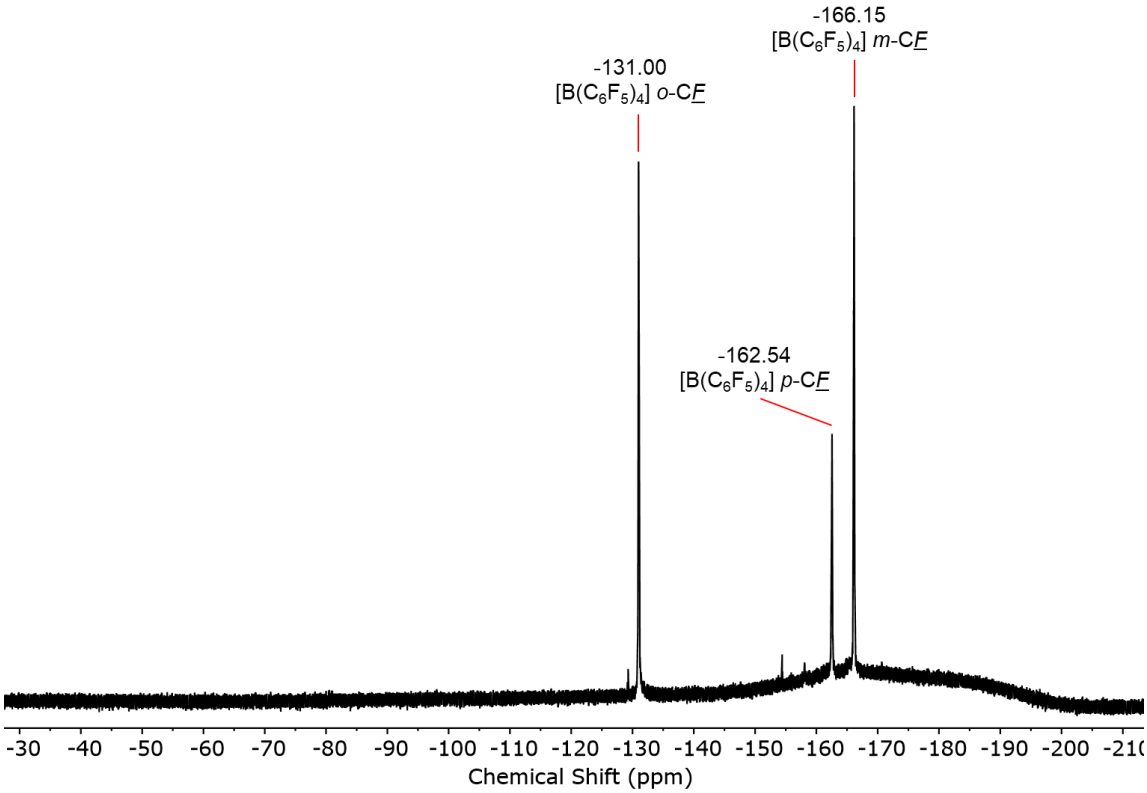

Figure S34. ^{19}F NMR spectrum of the reaction mixture between **3-Y** and $[CPh_3][B(C_6F_5)_4]$ in d_6-benzene.

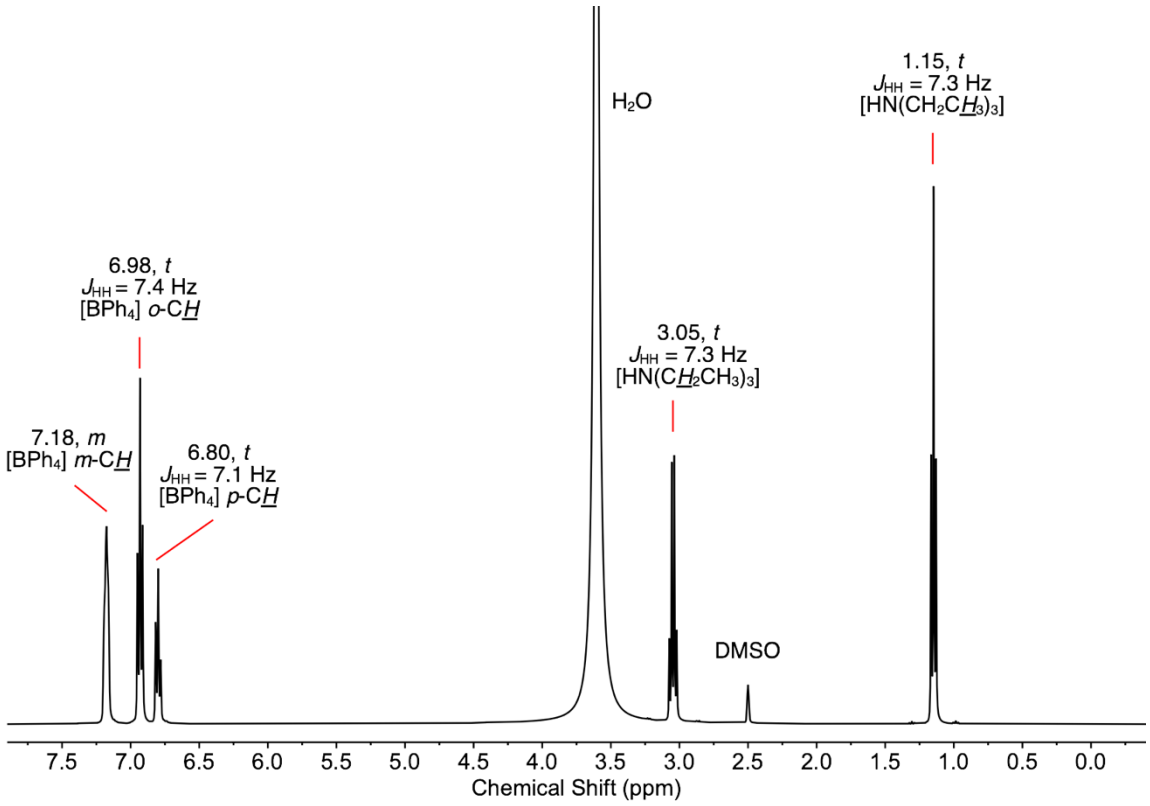

Figure S35. ^{1}H NMR spectrum of $[NEt_3H][BPh_4]$ in d_6-DMSO.

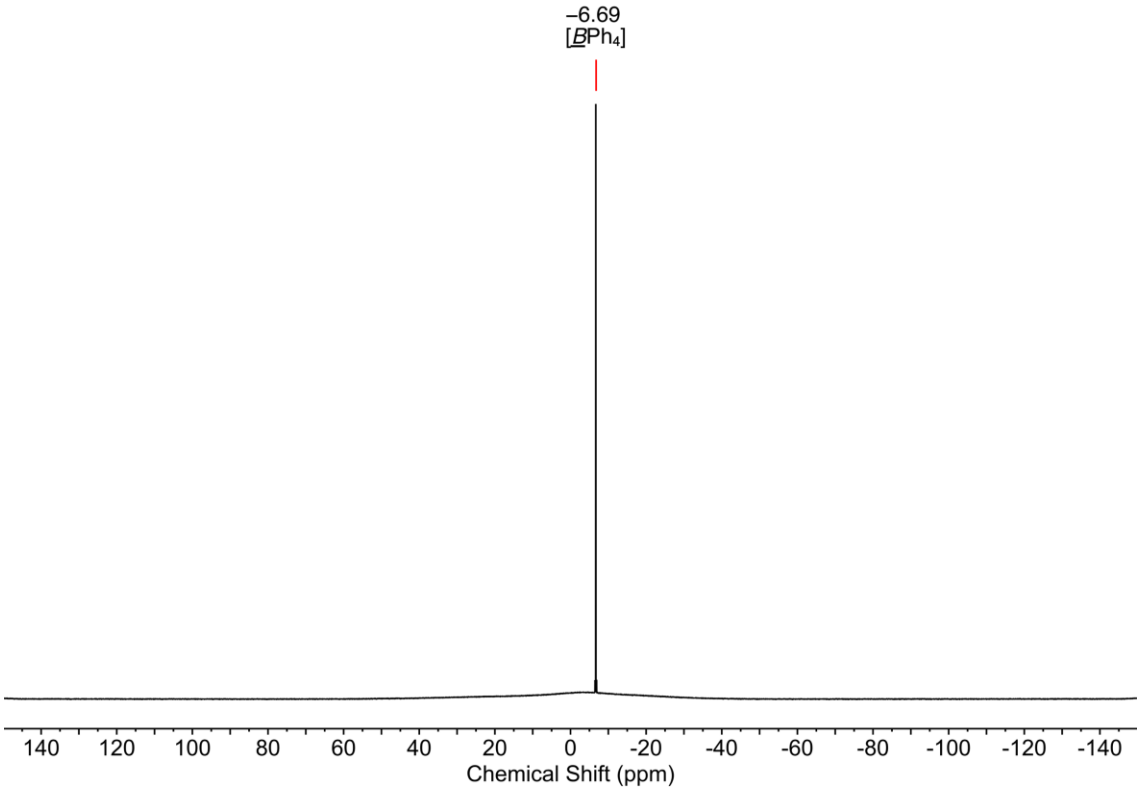

Figure S36. $^{11}B\{^{1}H\}$ NMR spectrum of $[NEt_3H][BPh_4]$ in d_6-DMSO.

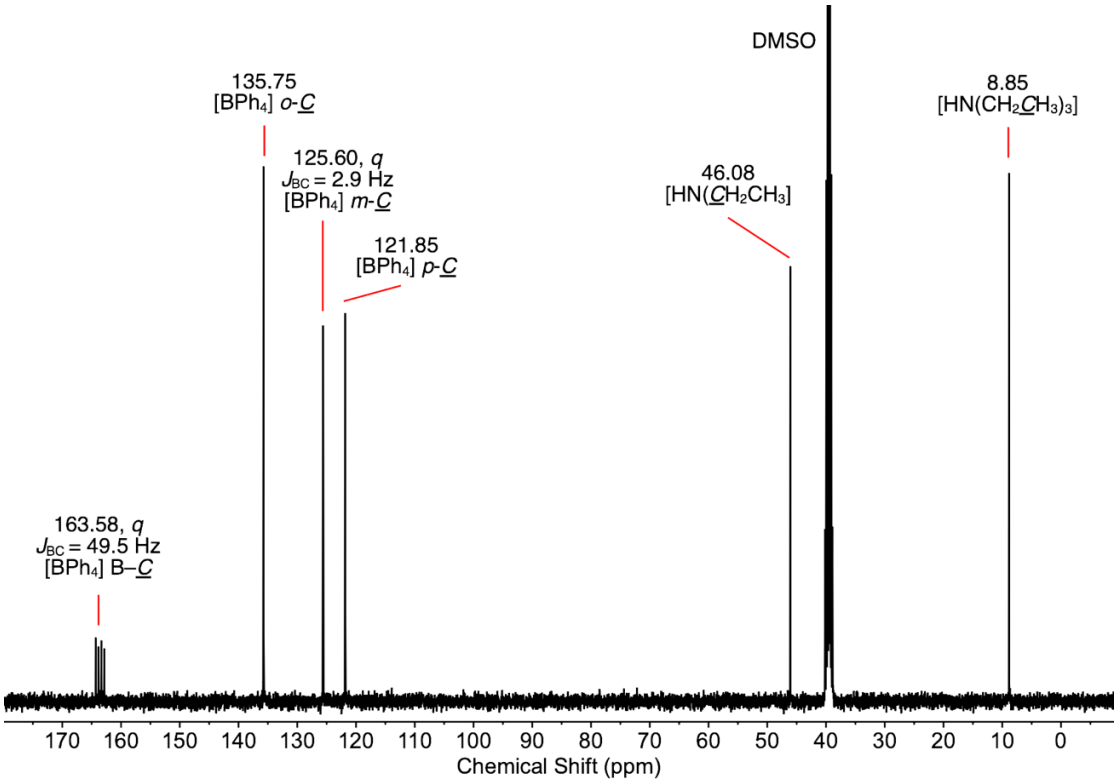

Figure S37. $^{13}C\{^{1}H\}$ NMR spectrum of $[NEt_3H][BPh_4]$ in d_6-DMSO.

3. FTIR spectroscopic data for 1-6 and [NEt_3H][BPh_4]

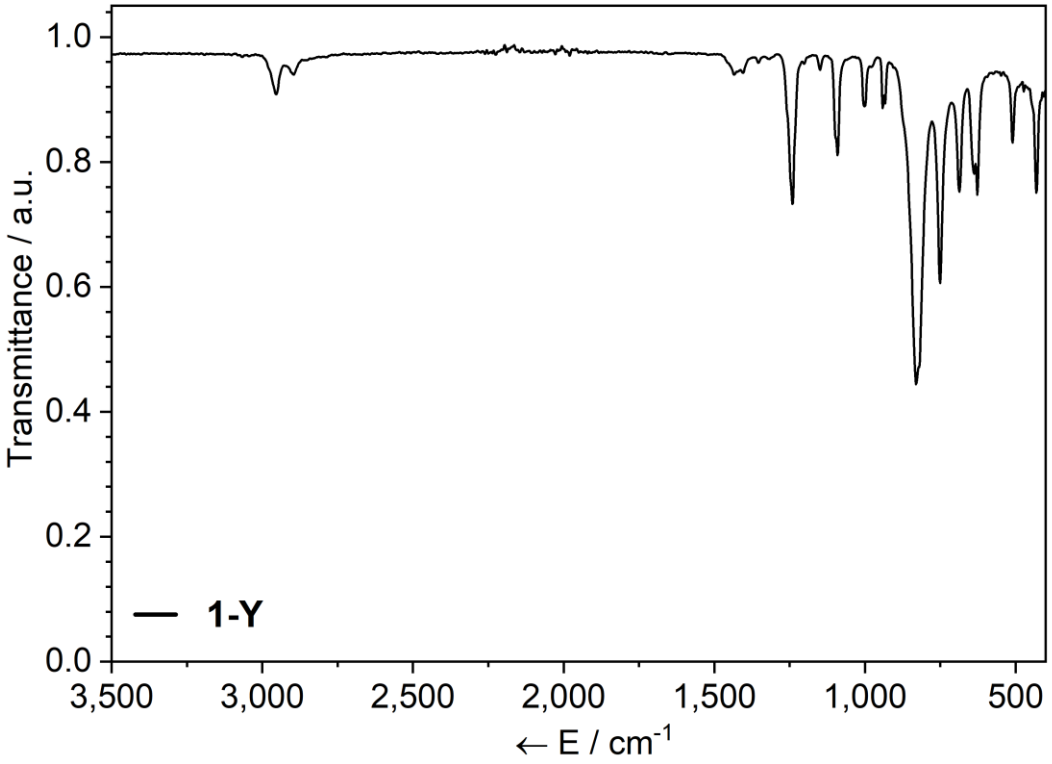

Figure S38. FTIR spectrum of **1-Y** (ATR-IR, microcrystalline powder).

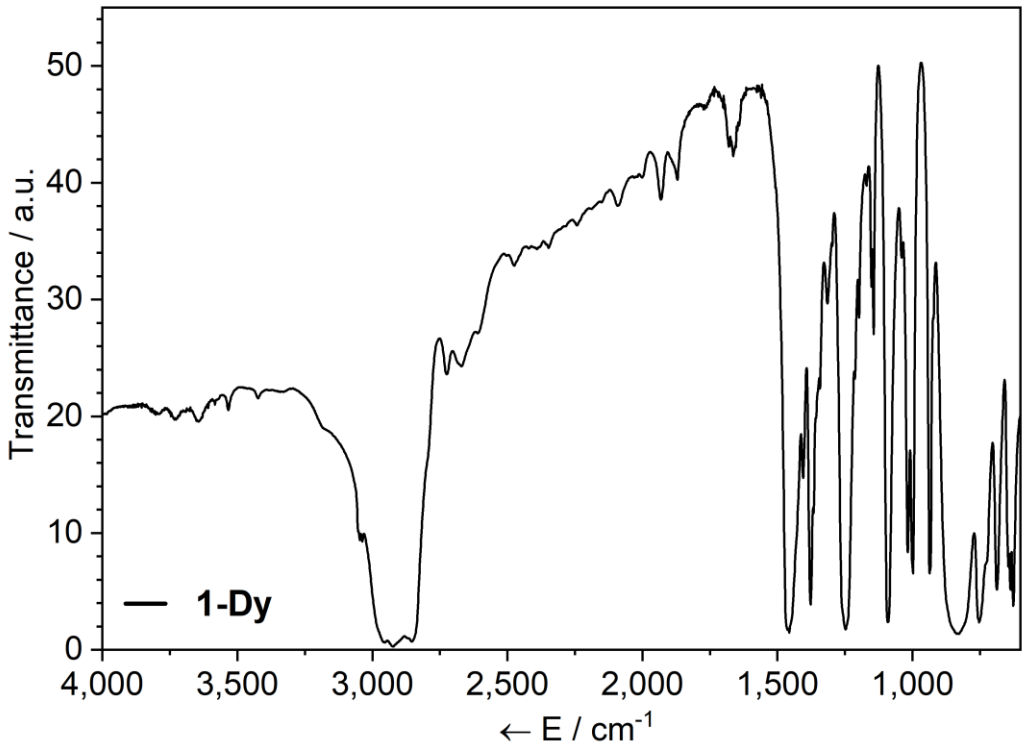

Figure S39. FTIR spectrum of **1-Dy** (Nujol mull, KBr discs).

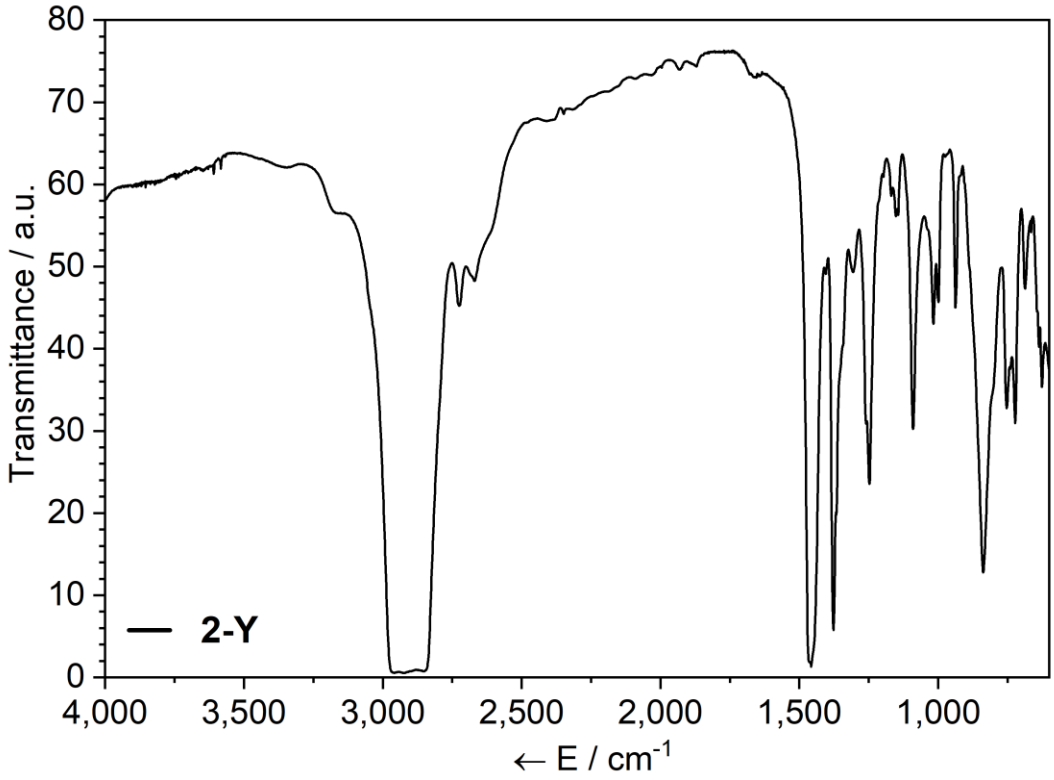

Figure S40. FTIR spectrum of **2-Y** (Nujol mull, KBr discs).

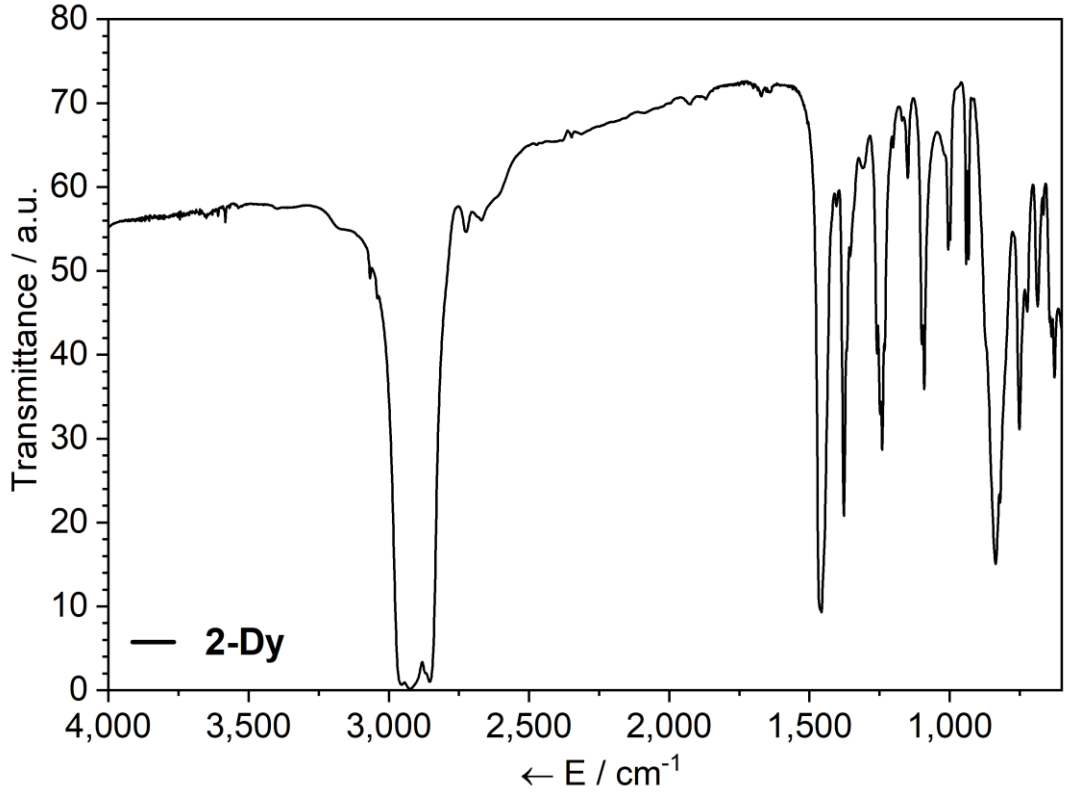

Figure S41. FTIR spectrum of **2-Dy** (Nujol mull, KBr discs).

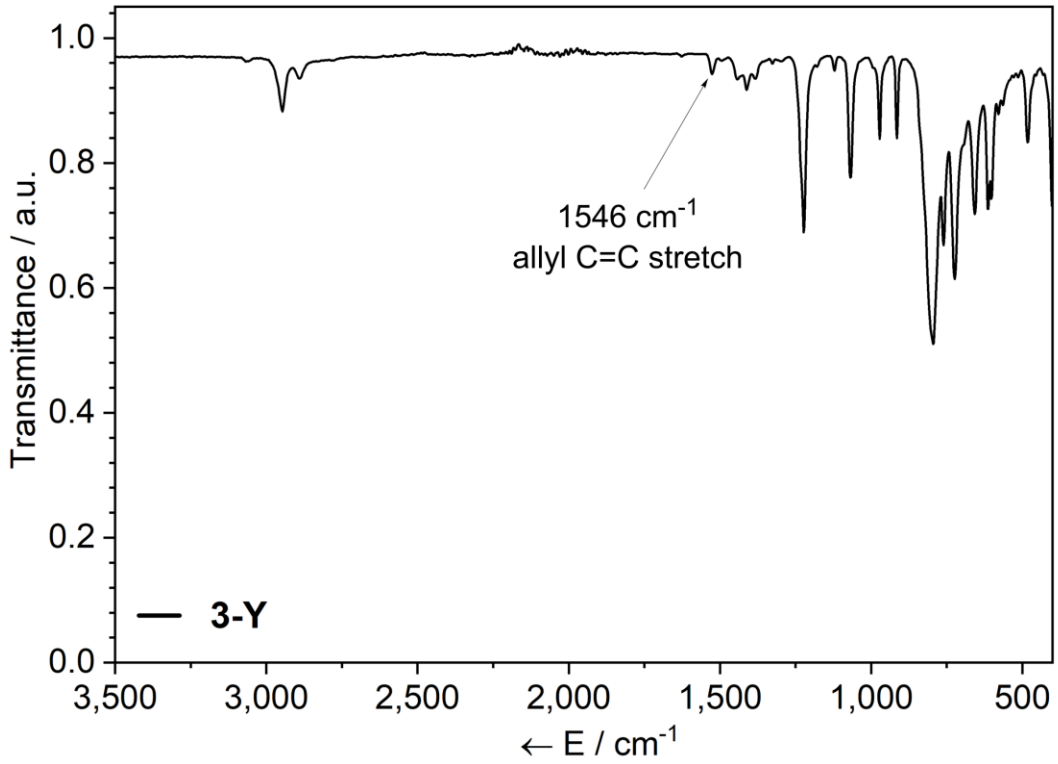

Figure S42. ATR-IR spectrum of **3-Y**.

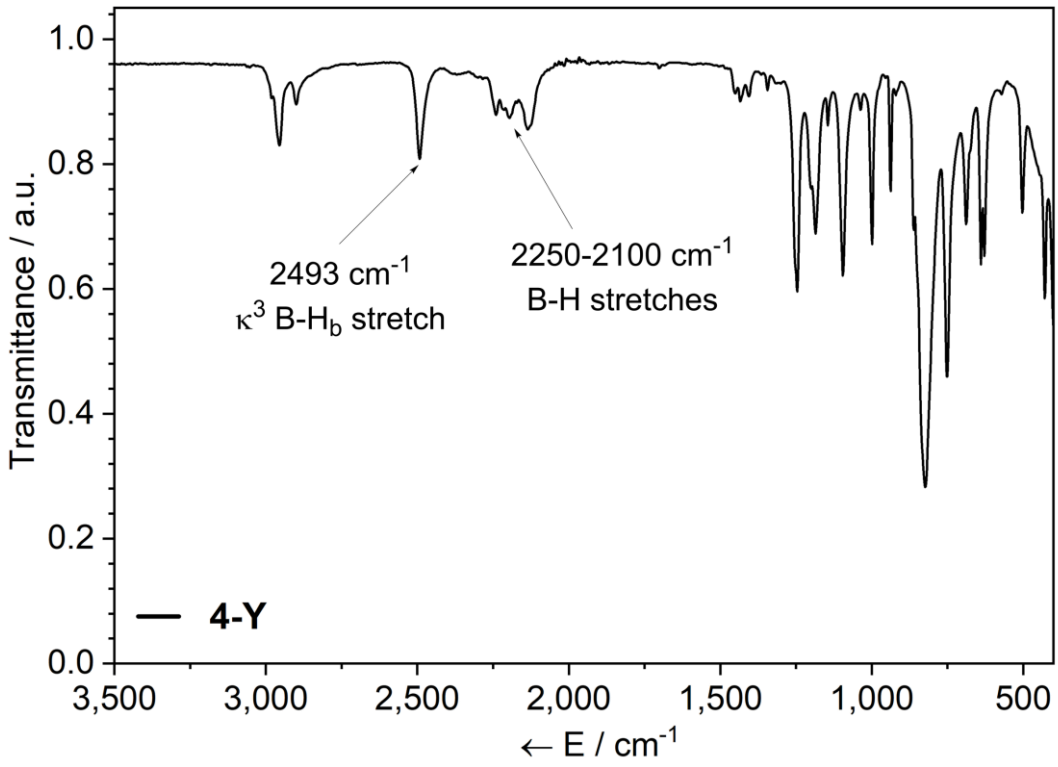

Figure S43. ATR-IR spectrum of **4-Y**.

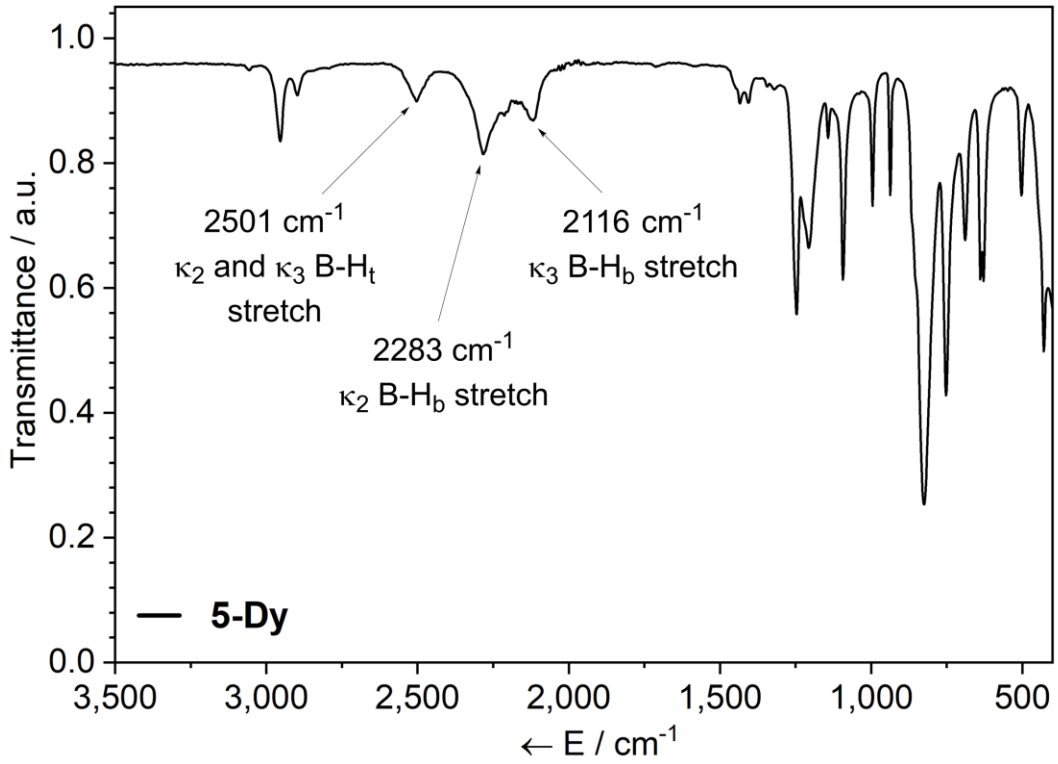

Figure S44. ATR-IR spectrum of **5-Dy**.

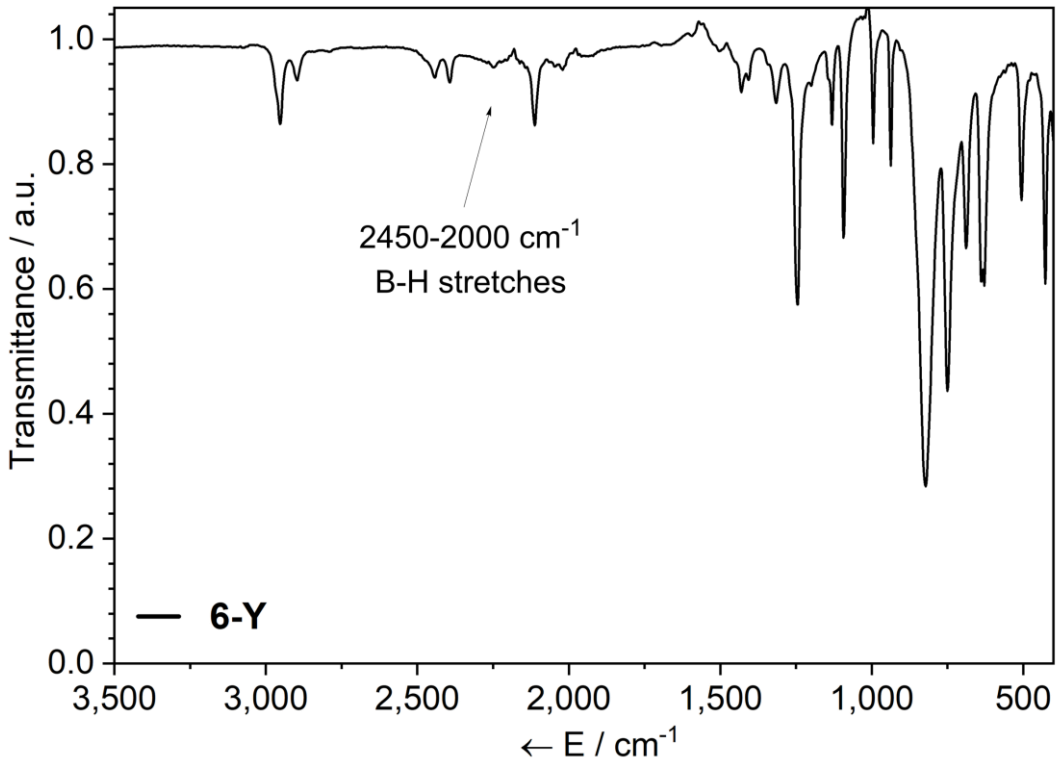

Figure S45. ATR-IR spectrum of **6-Y**.

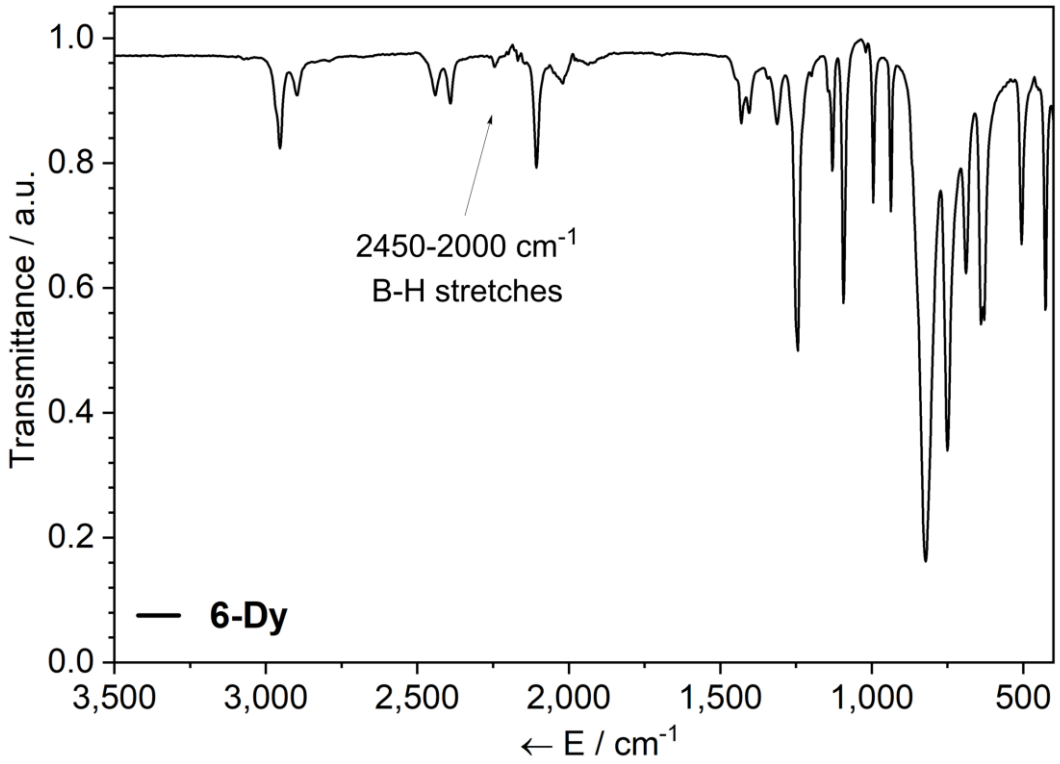

Figure S46. ATR-IR spectrum of **6-Dy**.

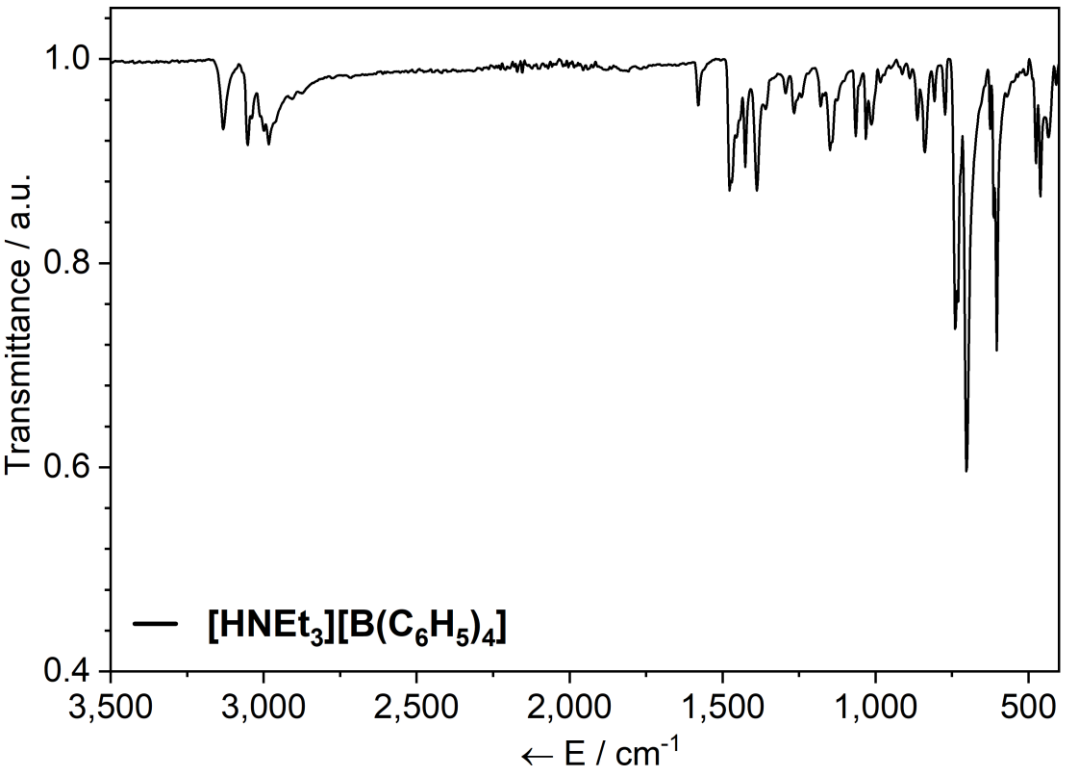

Figure S47. ATR-IR spectrum of $[NEt_3H][BPh_4]$.

4. X-ray Crystallography crystallographic data for 1-8, $[NEt_3H][BPh_4]$ and $[Mg(Cp'''')(THF)(\mu\text{-}Cl)]_2$

Crystal data for complexes **1-8**, $[NEt_3H][BPh_4]\cdot THF$ and $[Mg(Cp'''')(THF)(\mu\text{-}Cl)]_2\cdot C_6H_{14}$ are compiled in Tables S1-S5. Crystal data for **1-Dy** and **2-Dy** were collected on an Oxford Diffraction Xcalibur2 diffractometer, equipped with 4-circle kappa geometry goniometer, an Atlas CCD area detector, a sealed tube graphite monochromated MoKα radiation (λ = 0.71073 Å) source and an Oxford Instruments Cryojet, set at a temperature of 150 K. Crystal data for **4-Y**, $[NEt_3H][BPh_4]\cdot THF$ and $[Mg(Cp'''')(THF)(\mu\text{-}Cl)]_2\cdot C_6H_{14}$ were collected on an Oxford Diffraction Supernova diffractometer, equipped with 4-circle kappa geometry goniometer, an Eos CCD area detector, a microfocus source with MoKα radiation (λ = 0.71073 Å) and an Oxford Cryosystems Cryostream 700, set at a temperature of 150 K. Crystal data for **1-Y**, **2-Y**, **3-Y·C$_6$H$_{14}$**, **5-Dy**, **6-Dy**, **6-Y**, **7-Dy** and **8-Y** were collected on a Rigaku FR-X DW diffractometer equipped with an AFC-11 4-circle goniometer HyPix 6000HE photon counting pixel array detector, a microfocus rotating anode source, with Mo Kα radiation (λ = 0.71073 Å) (**3-Y·C$_6$H$_{14}$**) or Cu Kα radiation (λ = 1.54178 Å) (**1-Y**, **2-Y**, **5-Dy**, **6-Y**, **6-Dy**, **7-Dy** and **8-Y**) and an Oxford Cryosystems Cryostream 800, set at a temperature of 100 K (**2-Y** and **3-Y·C$_6$H$_{14}$**) or 150 K (**1-Y**, **5-Dy**, **6-Y**, **6-Dy**, **7-Dy** and **8-Y)**. A multi-scan absorption correction was applied for **1-Y**, **2-Y**, **6-Y** and **7-Dy**, whereas a Gaussian grid face-indexed absorption correction with a beam profile correction was applied for **1-Dy**, **2-Dy**, **3-Y·C$_6$H$_{14}$**, **4-Y**, **5-Dy**, **6-Dy**, **8-Y**, $[NEt_3H][BPh_4]\cdot THF$ and $[Mg(Cp'''')(THF)(\mu\text{-}Cl)]_2\cdot C_6H_{14}$. The structures were solved by direct methods and were refined by full-matrix least-squares on all unique F^2 values, with anisotropic displacement parameters for all non-hydrogen atoms, and with constrained riding hydrogen geometries. CrysAlisPro[2] was used for control and integration, and SHELX-20XX[3,4] was employed through OLEX2[5] for structure solution and refinement. ORTEP-3[6] and POVRAY[7] were used for molecular graphics.

Table S1. Crystal data for **1-Dy**, **1-Y** and **1a-Y**.

[a]Conventional $R = \Sigma||F_o| - |F_c||/\Sigma|F_o|$; $R_w = [\Sigma w(F_o^2 - F_c^2)^2/\Sigma w(F_o^2)^2]^{1/2}$; $S = [\Sigma w(F_o^2 - F_c^2)^2/\text{no. data} - \text{no. params})]^{1/2}$ for all data.

	1-Dy	**1-Y**	**1a-Y**
Formula	$C_{56}H_{116}Cl_4Dy_2K_2Si_{12}$	$C_{56}H_{116}Cl_4K_2Si_{12}Y_2$	$C_{56}H_{116}Cl_4K_2Si_{12}Y_2$
Fw	1671.56	1524.38	1524.38
Temperature, K	150.00(10)	150.00(10)	150.00(10)
Crystal size, mm	0.141 × 0.084 × 0.065	0.425 × 0.102 × 0.067	0.425 × 0.102 × 0.067
Crystal system	monoclinic	monoclinic	triclinic
Space group	$P2_1/n$	$P2_1/n$	$P\bar{1}$
a, Å	11.0500(7)	11.05270(10)	11.0201(5)
b, Å	16.0860(11)	16.0815(2)	12.1921(11)
c, Å	23.5320(18)	23.5252(3)	16.0564(9)
α, °			81.714(7)
β, °	101.589(7)	101.6330(10)	89.858(4)
γ, °			74.331(7)
V, Å^3	4097.5(5)	4095.57(8)	2054.0(2)
Z	2	2	1
ρ_{calc}, g/cm^3	1.355	1.236	1.232
μ, mm^{-1}	2.248	5.914	5.896
F(000)	1716	1608	804
No. of reflection (uniq.)	15047 (7524)	20846 (6384)	5720 (2877)
Rint	0.148	0.038	0.133
Data/restraints/parameters	7524/626/361	6384/0/361	2877/626/361
S[a]	0.97	1.08	1.14
R_1 (wR_2)($F^2>2\sigma(F^2)$)	0.1012 (0.1488)	0.0459 (0.1204)	0.1325 (0.3793)
R_1 (wR_2) All Data	0.2058 (0.1916)	0.0505 (0.1246)	0.1679 (0.4061)
min./max. diff map, e Å^{-3}	1.29/-1.46	1.15/-0.68	0.41/-0.56

Table S2. Crystal data for **2-Dy**, **2-Y** and **3-Y**.

[a]Conventional $R = \Sigma||F_o| - |F_c||/\Sigma|F_o|$; $R_w = [\Sigma w(F_o^2 - F_c^2)^2/\Sigma w(F_o^2)^2]^{1/2}$; $S = [\Sigma w(F_o^2 - F_c^2)^2/\text{no. data} - \text{no. params})]^{1/2}$ for all data.

	2-Dy	**2-Y**	**3-Y**
Formula	$C_{32}H_{66}ClDyOSi_6$	$C_{32}H_{66}ClOSi_6Y$	$C_{37}H_{77}Si_6Y$
Fw	833.33	759.74	779.43
Temperature, K	150.0(2)	100.0(2)	99.98(2)
Crystal size, mm	0.377 × 0.251 × 0.191	0.135 × 0.072 × 0.065	0.589 × 0.232 × 0.203
Crystal system	monoclinic	monoclinic	triclinic
Space group	$P2_1/c$	$P2_1/c$	$P\bar{1}$
a, Å	16.6630(5)	16.47510(10)	10.9184(3)
b, Å	13.2108(4)	13.16310(10)	12.8213(3)
c, Å	20.1131(6)	20.11540(10)	17.0002(4)
α, °			88.0069(19)
β, °	94.233(3)	94.1510(10)	83.231(2)
γ, °			76.864(2)
V, Å^3	4415.4(2)	4350.85(5)	2301.32(10)
Z	4	4	2
ρ_{calc}, g/cm^3	1.254	1.16	1.125
μ, mm^{-1}	1.937	4.191	1.446
F(000)	1732	1624	844
No. of reflection (uniq.)	27776 (10383)	47250 (8997)	27379 (8406)
Rint	0.038	0.043	0.065
Data/restraints/parameters	10383/383/465	8997/2420/749	8406/0/427
S^a	1.03	1.08	1.05
R_1 (wR_2)($F^2 > 2\sigma(F^2)$)	0.0342 (0.0603)	0.0330 (0.0814)	0.0546 (0.1469)
R_1 (wR_2) *All Data*	0.0508 (0.0669)	0.0366 (0.0831)	0.0623 (0.1515)
min./max. diff map, e Å^{-3}	0.90/-0.71	0.72/-0.67	2.16/-0.60

Table S3. Crystal data for **5-Dy**, **6-Dy** and **6-Y**.

[a]Conventional $R = \Sigma||F_o| - |F_c||/\Sigma|F_o|$; $R_w = [\Sigma w(F_o^2 - F_c^2)^2/\Sigma w(F_o^2)^2]^{1/2}$; $S = [\Sigma w(F_o^2 - F_c^2)^2/\text{no. data} - \text{no. params})]^{1/2}$ for all data.

	4-Y	**5-Dy**	**6-Dy**
Formula	$C_{18}H_{45}B_2OSi_3Y$	$C_{56}H_{148}B_8Dy_4Si_{12}$	$C_{28}H_{62}BDySi_6$
Fw	472.34	1895.3	740.62
Temperature, K	150(2)	149.99(10)	150.00(10)
Crystal size, mm	0.26 × 0.177 × 0.074	0.146 × 0.101 × 0.058	0.298 × 0.215 × 0.189
Crystal system	monoclinic	triclinic	monoclinic
Space group	$P2_1/n$	P–1	$P2_1$
a, Å	13.0628(10)	11.7394(4)	10.85530(15)
b, Å	12.6435(13)	15.4866(6)	16.84522(19)
c, Å	17.2075(15)	57.0982(12)	11.34382(15)
α, °		88.431(2)	
β, °	102.680(9)	87.394(2)	108.4482(15)
γ, °		68.254(3)	
V, Å^3	2772.7(4)	9631.3(6)	1967.73(5)
Z	4	4	2
$\rho_{calc,}$ g/cm^3	1.132	1.307	1.25
μ, mm^{-1}	2.238	17.938	12.006
F(000)	1008	3824	770
No. of reflection (uniq.)	9085 (5028)	62038 (20111)	41794 (7142)
Rint	0.081	0.111	0.040
Data/restraints/parameters	5028/290/267	20111/364/1566	7142/5/355
S^a	1.03	1.1	1.06
R_1 (wR_2)($F^2 > 2\sigma(F^2)$)	0.0745 (0.1323)	0.0670 (0.1694)	0.0256 (0.0706)
R_1 (wR_2) *All Data*	0.1461 (0.1741)	0.0927 (0.1839)	0.0258 (0.0707)
min./max. diff map, e Å^{-3}	0.96/-0.97	1.71/-1.96	0.61/-0.70
Flack parameter		-0.003(2)	-0.027(3)

Table S4. Crystal data for **6-Y**, **7-Dy** and **8-Y**.

[a]Conventional $R = \Sigma||F_o| - |F_c||/\Sigma|F_o|$; $R_w = [\Sigma w(F_o^2 - F_c^2)^2/\Sigma w(F_o^2)^2]^{1/2}$; $S = [\Sigma w(F_o^2 - F_c^2)^2/\text{no. data} - \text{no. params})]^{1/2}$ for all data.

	6-Y	**7-Dy**	**8-Y**
Formula	$C_{28}H_{62}BSi_6Y$	$C_{32}H_{70}BDyOSi_6$	$C_{52}H_{78}BSi_6Y$
Fw	667.03	812.73	971.4
Temperature, K	150(2)	150.07(10)	150(2)
Crystal size, mm	0.367 × 0.155 × 0.151	0.209 × 0.145 × 0.122	0.148 × 0.123 × 0.106
Crystal system	monoclinic	monoclinic	triclinic
Space group	$P2_1$	$P2_1/c$	$P\bar{1}$
a, Å	10.83339(8)	16.8987(3)	12.52981(18)
b, Å	16.83695(10)	13.0779(2)	21.5621(3)
c, Å	11.33098(8)	20.2904(3)	23.3261(4)
α, °			64.3568(16)
β, °	108.3363(8)	93.1940(10)	77.9174(13)
γ, °			80.8704(13)
V, Å^3	1961.85(2)	4477.20(12)	5538.85(17)
Z	2	4	4
ρ_{calc}, g/cm^3	1.129	1.206	1.165
μ, mm^{-1}	3.947	10.613	2.953
F(000)	716	1700	2072
No. of reflection (uniq.)	22451 (7159)	51395 (8196)	86762 (20083)
Rint	0.0157	0.0801	0.0386
Data/restraints/parameters	7159/5/355	8196/119/440	20083/0/1117
S^a	1.03	1.09	1.03
R_1 (wR_2)($F^2 > 2\sigma(F^2)$)	0.0160 (0.0422)	0.0454 (0.1204)	0.0330 (0.0817)
R_1 (wR_2) *All Data*	0.0162 (0.0423)	0.0533 (0.1248)	0.0387 (0.0844)
min./max. diff map, e Å^{-3}	0.24/-0.33	0.79/-1.83	0.59/-0.59

Table S5. Crystal data for $[NEt_3H][BPh_4]\cdot THF$ and $[Mg(Cp''')(THF)(\mu\text{-}Cl)]_2\cdot C_6H_{14}$.

[a]Conventional $R = \Sigma||F_o| - |F_c||/\Sigma|F_o|$; $R_w = [\Sigma w(F_o^2 - F_c^2)^2/\Sigma w(F_o^2)^2]^{1/2}$; $S = [\Sigma w(F_o^2 - F_c^2)^2/\text{no. data} - \text{no. params})]^{1/2}$ for all data.

	$[NEt_3H][BPh_4]\cdot THF$	$[Mg(Cp''')(THF)(\mu\text{-}Cl)]_2\cdot C_6H_{14}$
Formula	$C_{34}H_{44}BNO$	$C_{42}H_{88}Cl_2Mg_2O_2Si_6$
Fw	493.51	913.18
Temperature, K	100(2)	150(2)
Crystal size, mm	0.198 × 0.424 × 0.667	0.147 × 0.228 × 0.242
Crystal system	monoclinic	triclinic
Space group	$P2_1/c$	$P\text{–}1$
a, Å	28.936(3)	11.3143(7)
b, Å	18.392(2)	11.4487(7)
c, Å	16.501(2)	12.8059(8)
α, °		65.240(6)
β, °	97.868(11)	66.971(6)
γ, °		84.947(5)
V, Å^3	8699.0(17)	1380.56(16)
Z	12	1
ρ_{calcd}, g cm^3	1.130	1.098
μ, mm^{-1}	0.066	0.301
F(*000*)	3216	498
No. of reflections (uniq.)	13734 (6649)	8027 (5008)
Rint	0.091	0.031
Data/restraints/parameters	17524/0/1009	5008/237/254
S[a]	0.97	1.03
$R_1(wR_2)$ ($F^2 > 2\sigma(F^2)$)	0.0552 (0.1357)	0.0681 (0.1676)
R1 (wR2) All Data	0.0753 (0.1479)	0.0977 (0.1880)
min./max. diff map, e Å^{-3}	–0.294, 0.326	–0.44, 1.54

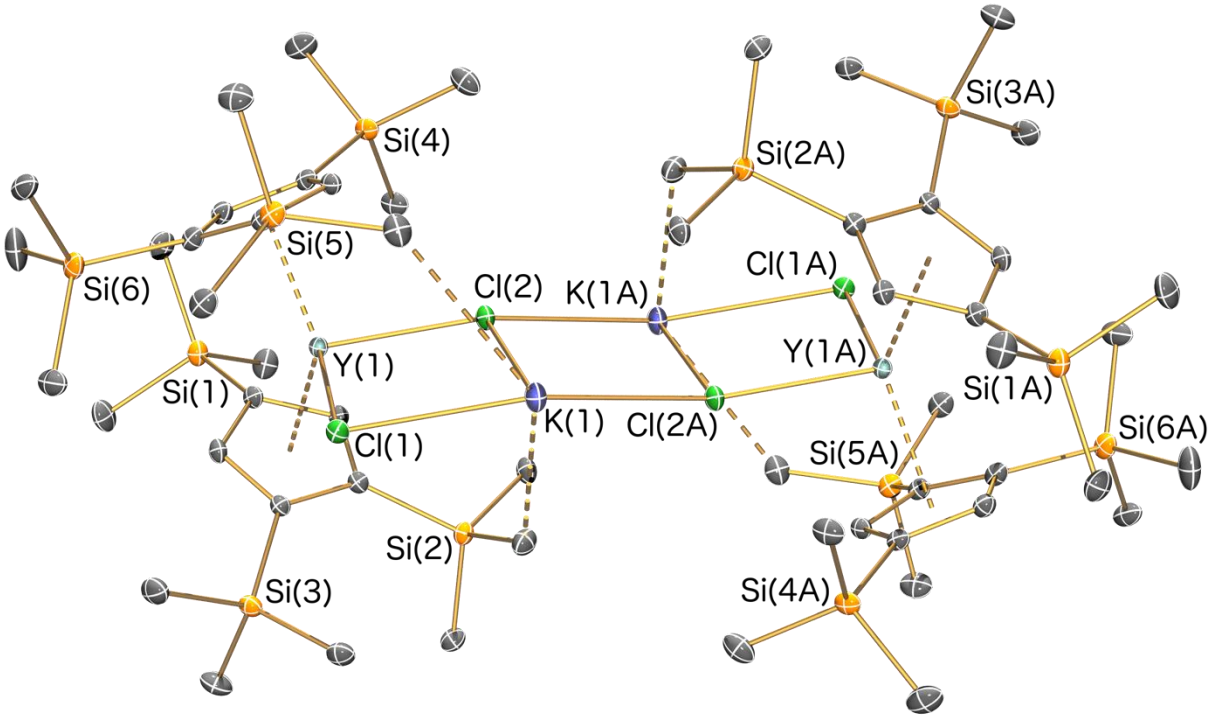

Figure S48. Molecular structure of $[\{Y(Cp''')_2(\mu\text{-}Cl)_2K\}_2]_\infty$ (**1-Y**) with selective atom labelling. Displacement ellipsoids set at 30 % probability level and hydrogen atoms omitted for clarity. Symmetry operation to generate equivalent atoms: $2 - x$, $1 - y$, $1 - z$.

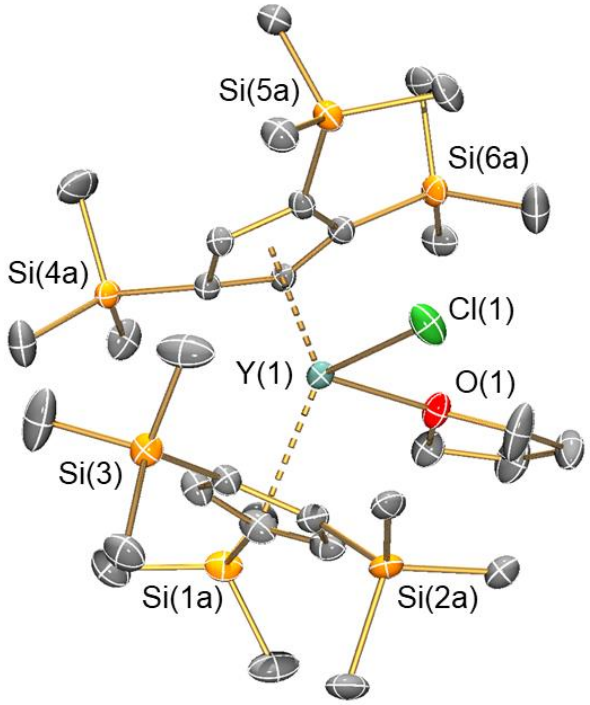

Figure S49. Molecular structure of $[Y(Cp''')_2(THF)(Cl)]$ (**2-Y**) with selective atom labelling. Displacement ellipsoids set at 30 % probability level and hydrogen atoms and modelled disorder components omitted for clarity.

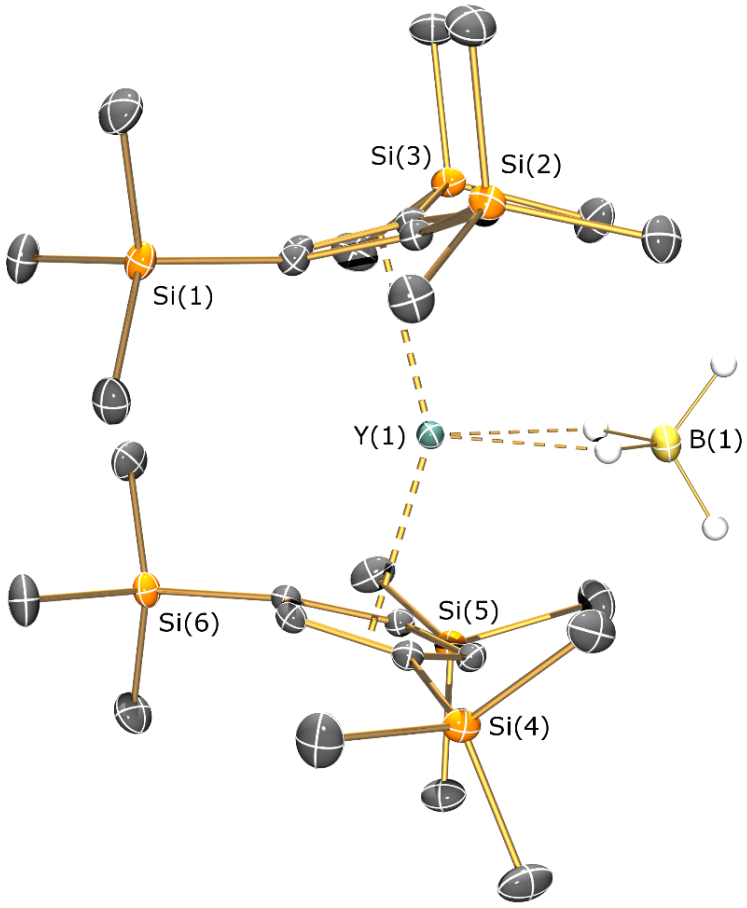

Figure S50. Molecular structure of [Y(Cp‴)$_2$(BH$_4$)] (**6-Y**) with selective atom labelling. Displacement ellipsoids set at 30 % probability level and hydrogen atoms omitted for clarity, with the exception of those belonging to the borohydride group.

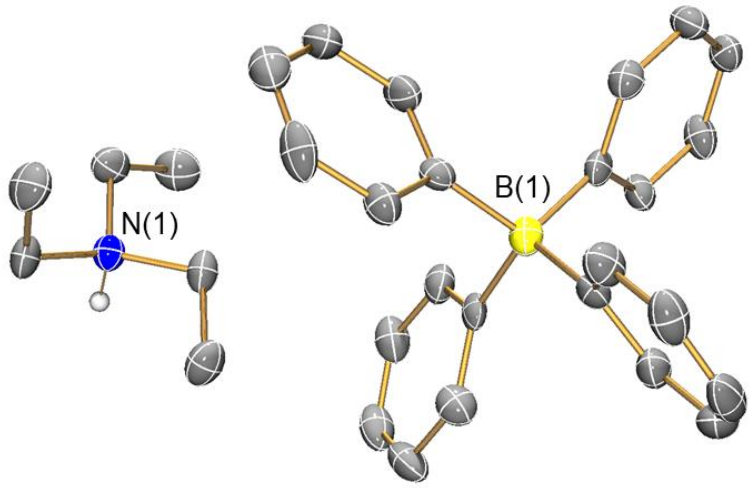

Figure S51. Molecular structure of [NEt$_3$H][BPh$_4$]·THF with selective atom labelling. Displacement ellipsoids set at 30 % probability level and hydrogen atoms and lattice solvent omitted for clarity.

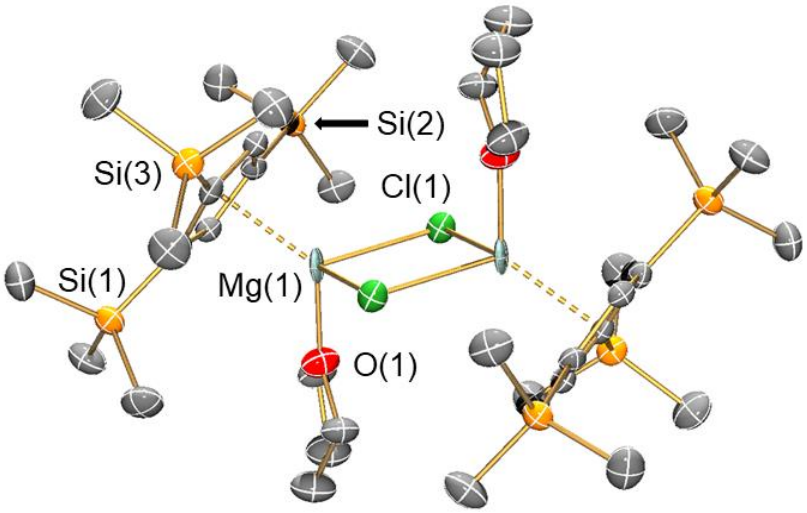

Figure S52. Molecular structure of [Mg(Cp‴)(THF)(μ-Cl)]$_2$ with selective atom labelling. Displacement ellipsoids set at 30 % probability level and hydrogen atoms omitted for clarity. Symmetry operation to generate equivalent atoms: $-x, -y, 1-z$.

5. Magnetic data for 5-Dy

Magnetic measurements were performed on a Quantum Design MPMS3 superconducting quantum interference device (SQUID) magnetometer. The sample of **5-Dy** (19.1 mg) was ground to a powder, loaded in a borosilicate glass NMR tube and covered in ground eicosane (9.7 mg) in a glovebox. The tube was removed from the glovebox, kept under a protected atmosphere and transferred onto a Schlenk line, where the eicosane powder was melted under an argon atmosphere. The NMR tube was then sealed at ~3 cm under reduced pressure. Kapton tape was wrapped around the top of the tube, the NMR tube was held inside a straw by friction, and the straw was attached to the end of the sample rod.

All dc measurements were taken in dc scan mode with a 40 mm scan length and scan time of 60 s. The raw data were corrected for the diamagnetic contribution of the sample holder and eicosane using calibrated blanks. The data were corrected for the sample shape using the Quantum Design MPMS3 Geometry Simulator, assuming a uniform cylinder of 4.06 mm diameter and 3.58 mm height. Finally the data were corrected for the intrinsic diamagnetic contribution of the sample, estimated as the molecular weight (g/mol) multiplied by 0.5×10^{-6} $cm^3\,K\,mol^{-1}$.

The equilibrium susceptibility was measured on cooling in temperature settle mode, with rates of 5 K/min between 300 and 100 K, 2 K/min 100-10 K and 1 K/min below 10 K. The zero-field cooled (ZFC) and field cooled (FC) measurements were performed in temperature sweep mode with a sweep rate of 0.5 K/min and range 2-100 K. The ZFC sample was prepared by cooling from at least 100 K in zero field and holding at 2 K for 2.5 hrs before rapidly ramping the dc field at 700 Oe/s to 0.1 T and beginning the measurement on warming. The FC measurement was performed on cooling at the same rate. Hysteresis measurements were performed between +7 and -7 T in field sweep mode with sweep rates of 22 Oe/s between ±1 T, 54 Oe/s for 1-2 T and 91 Oe/s for 2-7 T. Magnetisation measurements were performed between 0-7 T at 2 and 4 K in field settle mode. The field was ramped at 500 Oe/s between points and held constant for at least 5 min before measuring (10 min at 2 K, 0-3.5 T). All ac data were collected with a five point measure, using an oscillating field amplitude of H_{ac} = 2 Oe. Data were collected at 8 log-spaced frequencies per decade in the range 0.1-1000 Hz, averaging over 2 sec or 10 cycles, whichever was longer.

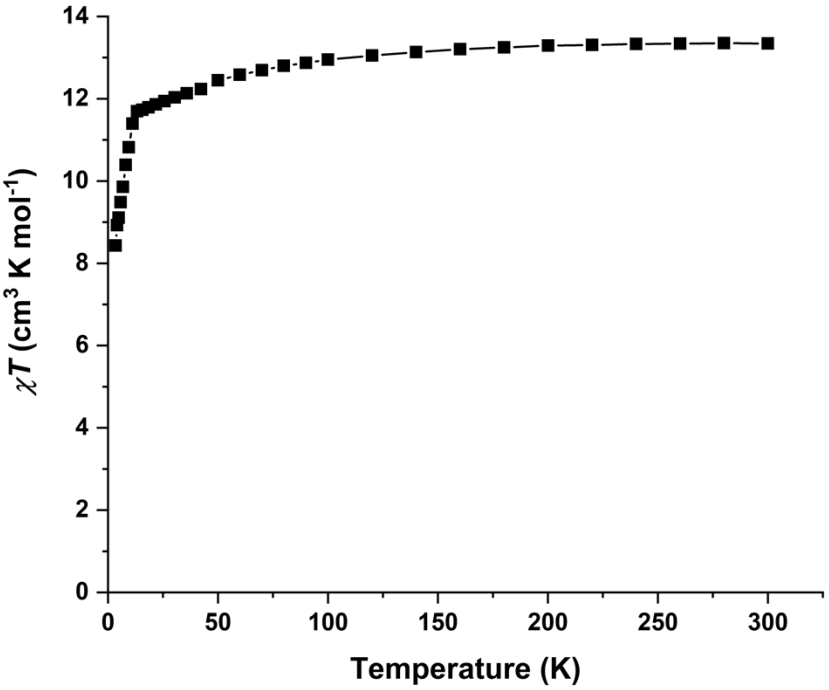

Figure S53. Temperature dependence of the product of magnetic susceptibility and temperature (χT) for **5-Dy**, reported per Dy ion.

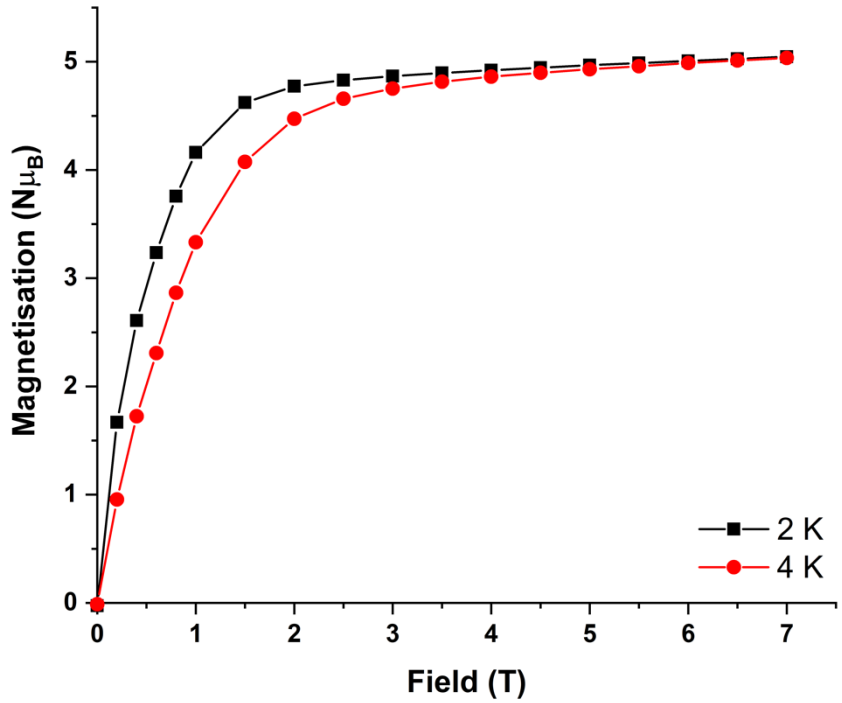

Figure S54. Magnetisation vs. field at 2 K (black) and 4 K (red) for **5-Dy**, reported per Dy ion.

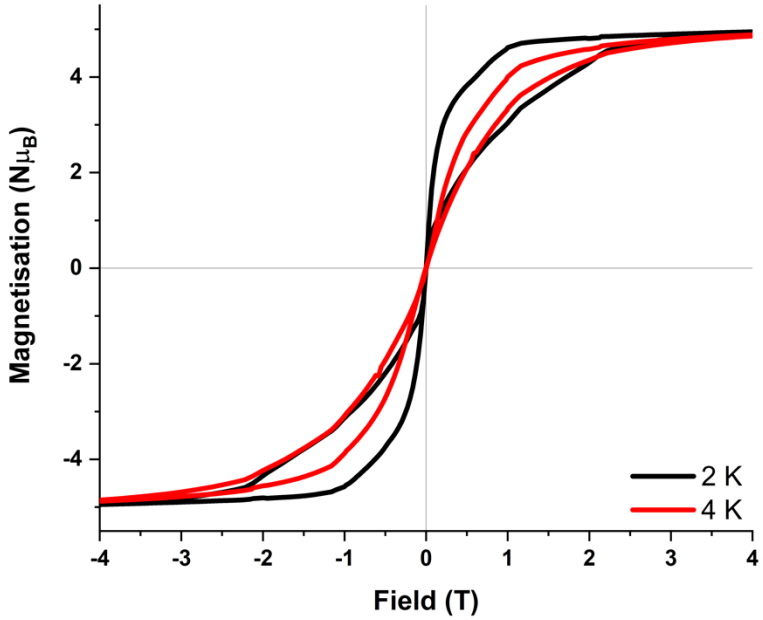

Figure S55. Hysteresis curve at 2 K (black) and 4 K (red) for **5-Dy**, reported per Dy ion. Points recorded in 250 Oe steps with sweep rates of 22 Oe/s for |H| < 1 T, 54 Oe/s for 1 < |H| < 2 T and 91 Oe/s for 2 < |H| < 7 T.

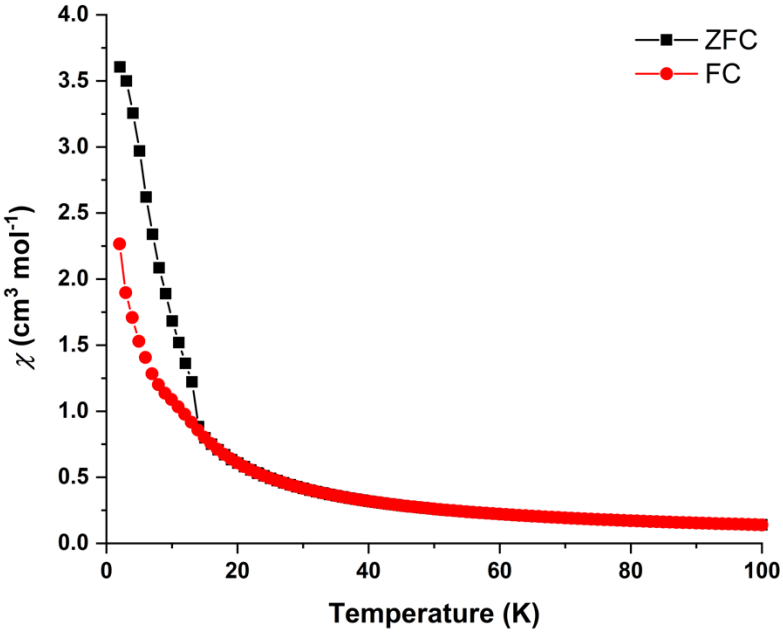

Figure S56. Zero-field cooled susceptibility measured on warming (black) and field-cooled susceptibility measured on cooling (red) for **5-Dy**, reported per Dy ion. Measurements performed for 2-100 K, recording points every 1 K and with a sweep rate of 0.5 K/min.

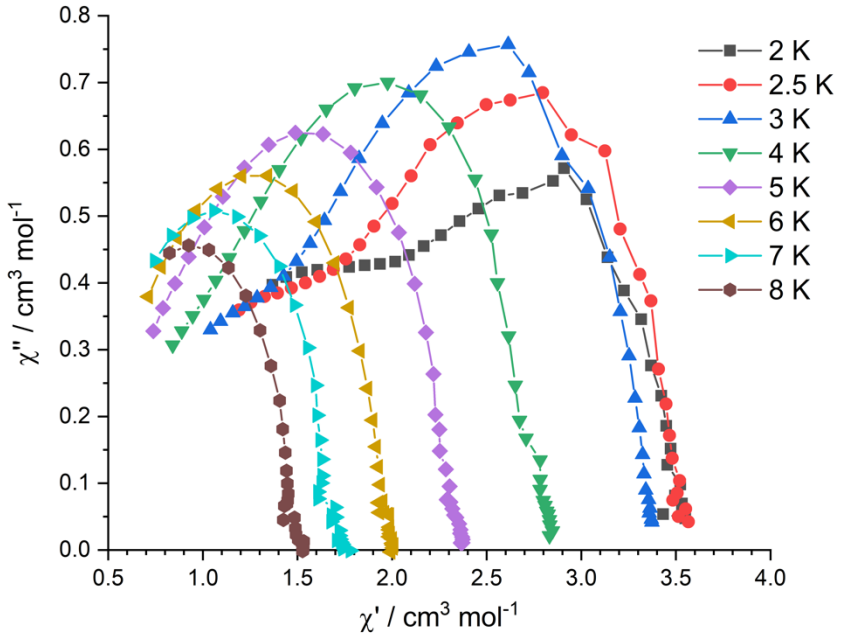

Figure S57. Cole-Cole plot for **5-Dy**, reported per Dy ion, at 2-8 K and measured in an applied field of 0.1 T. Lines are guides for the eye.

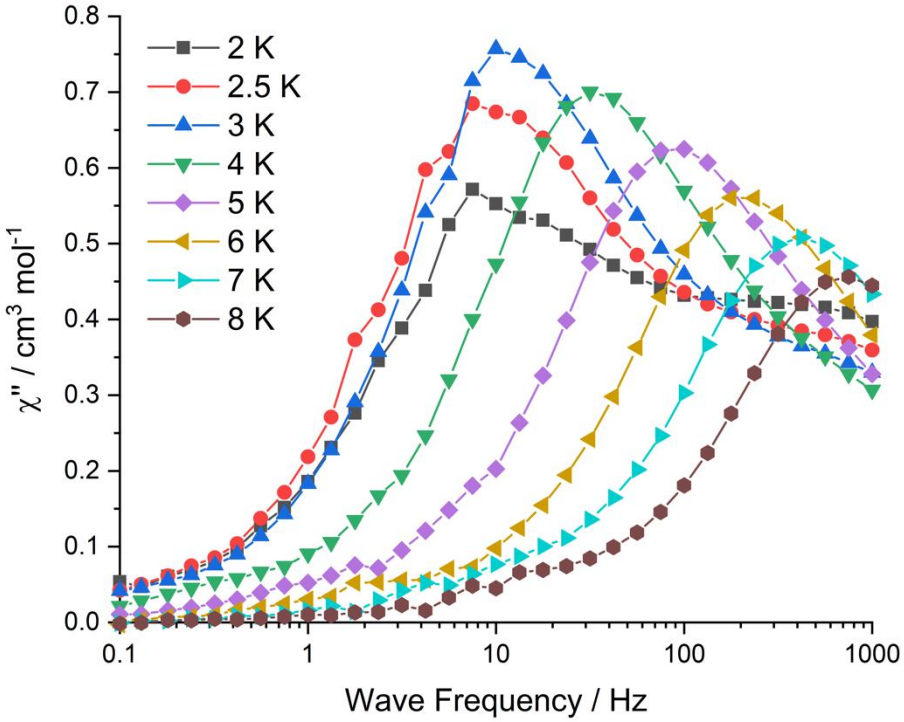

Figure S58. Frequency dependence of the out-of-phase susceptibility (χ″) per Dy ion for **5-Dy**, measured at 2-8 K in an applied field of 0.1 T. Lines are guides for the eye.

6. CASSCF-SO calculations for 5-Dy

OpenMolcas[8] was used to perform CASSCF-SO calculations on each $[Dy(Cp''')(BH_4)_3]^-$ unit of **5-Dy** to determine the electronic structures of the four independent Dy(III) ions. The molecular geometries from the single crystal XRD structure were used with no optimization, taking the largest disorder component only. Integrals were performed in the SEWARD module using basis sets from ANO-RCC library[9,10] with VTZP quality for Dy atoms, VDZP quality for the cyclopentadienyl C atoms and the borohydride B atoms and VDZ quality for all remaining atoms, employing the second-order DKH transformation. Cholesky decomposition of the two-electron integrals with a threshold of 10^{-8} was performed to save disk space and reduce computational demand. The molecular orbitals (MOs) were optimised in state-averaged CASSCF calculations in the RASSCF module, where the active space was defined by the nine 4f electrons in the seven 4f orbitals of Dy(III). Three such calculations were performed independently for each possible spin state, where 21 roots were included for S = 5/2, 224 roots were included for S = 3/2, and 490 roots were included for S = 1/2. The wavefunctions obtained from these CASSCF calculations were then mixed by spin orbit coupling in the RASSI module, where all 21 S = 5/2 states, the lowest 128 S = 3/2 states, and the lowest 130 S = 1/2 states were included. SINGLE_ANISO was used to decompose the resulting spin-orbit wave functions into the CF Hamiltonian formalism.[11] Diamond was employed for molecular graphics.[12]

Table S6. Electronic structure of $[Dy(Cp'''')(BH_4)_3]^-$ (where Dy(1) is the central ion) calculated with the crystal field parameters obtained from CASSCF-SO using the solid state geometry of **5-Dy** in zero-field. Each row corresponds to a Kramers doublet.

Energy (cm^{-1})	Energy (K)	g_x	g_y	g_z	Angle[a] (deg)	Wavefunction	$<J_z>$
0.00	0.00	0.0	0.0	19.8	--	98.9% |± 15/2⟩	±7.5
102.11	146.94	0.2	0.4	18.6	75.6	21% |± 5/2⟩ + 16% |∓ 7/2⟩ + 15% |± 9/2⟩ + 13% |∓ 3/2⟩ + 10% |± 1/2⟩ + 8% |± 7/2⟩ + 6% |∓ 11/2⟩	±3.1
148.08	213.08	1.8	2.1	15.6	26.2	46% |± 13/2⟩ + 22% |± 11/2⟩ + 14% |∓ 13/2⟩ + 5% |± 9/2⟩	±5.8
86.72	268.69	4.8	7.0	8.2	83.1	28% |± 9/2⟩ + 13% |∓ 7/2⟩ + 11% |± 13/2⟩ + 10% |∓ 11/2⟩ + 9% |∓ 13/2⟩ + 8% |± 11/2⟩ + 5% |± 7/2⟩	±4.6
218.05	313.77	0.1	0.7	18.2	84.5	26% |± 5/2⟩ + 25% |∓ 3/2⟩ + 20% |± 1/2⟩ + 12% |∓ 7/2⟩	±2.2
254.04	365.57	0.4	2.6	13.6	82.8	21% |± 1/2⟩ + 20% |∓ 7/2⟩ + 13% |± 9/2⟩ + 9% |± 11/2⟩ + 9% |∓ 11/2⟩ + 6% |∓ 5/2⟩ + 5% |± 3/2⟩ + 5% |∓ 3/2⟩	±3.2
284.25	409.04	0.9	2.5	16.2	64.7	17% |± 9/2⟩ + 17% |± 5/2⟩ + 15% |± 11/2⟩ + 12% |∓ 3/2⟩ + 11% |∓ 7/2⟩ + 7% |± 13/2⟩ + 7% |∓ 11/2⟩ + 7% |± 1/2⟩	±3.8
397.99	572.71	0.0	0.1	19.3	85.5	28% |± 3/2⟩ + 26% |∓ 3/2⟩ + 10% |∓ 5/2⟩ + 9% |± 1/2⟩ + 8% |± 7/2⟩ + 8% |± 5/2⟩ + 5% |∓ 9/2⟩	±1.9

[a] The angle between the g_z value of the excited Kramers doublet and the ground Kramers doublet.

Table S7. Electronic structure of $[Dy(Cp'')(BH_4)_3]^-$ (where Dy(2) is the central ion) calculated with the crystal field parameters obtained from CASSCF-SO using the solid state geometry of **5-Dy** in zero-field. Each row corresponds to a Kramers doublet.

Energy (cm^{-1})	Energy (K)	g_x	g_y	g_z	Angle[a] (deg)	Wavefunction	$<J_z>$
0.00	0.00	0.6	5.8	13.0	--	36% |± 15/2⟩ + 30% |± 11/2⟩ + 18% |± 7/2⟩	±5.4
16.10	23.17	1.4	3.9	12.3	42.1	25% |± 9/2⟩ + 15% |∓ 9/2⟩ + 14% |± 15/2⟩ + 10% |∓ 5/2⟩ + 9% |± 5/2⟩	±4.5
57.57	82.84	0.8	1.9	14.0	24.7	49% |± 13/2⟩ + 20% |± 7/2⟩ + 12% |± 11/2⟩ + 5% |± 3/2⟩	±5.3
97.73	140.64	1.6	4.3	9.9	74.3	19% |± 3/2⟩ + 16% |∓ 5/2⟩ + 11% |∓ 1/2⟩ + 9% |∓ 13/2⟩ + 8% |± 15/2⟩ + 7% |∓ 11/2⟩ + 6% |± 11/2⟩ + 5% |± 9/2⟩	±3.6
118.91	171.11	2.2	6.2	7.4	38.5	25% |± 15/2⟩ + 15% |± 9/2⟩ + 13% |± 11/2⟩ + 11% |∓ 9/2⟩ + 8% |∓ 11/2⟩ + 6% |∓ 5/2⟩ + 5% |∓ 13/2⟩ + 5% |∓ 1/2⟩	±5.0
137.99	198.57	0.5	4.3	6.5	46.0	17% |± 7/2⟩ + 16% |∓ 7/2⟩ + 12% |± 13/2⟩ + 9% |∓ 1/2⟩ + 8% |± 11/2⟩ + 8% |∓ 15/2⟩ + 7% |± 9/2⟩ + 7% |∓ 3/2⟩ + 5% |∓ 11/2⟩ + 5% |∓ 9/2⟩	±4.0
176.71	254.29	2.9	5.4	12.3	86.3	28% |± 5/2⟩ + 18% |∓ 1/2⟩ + 10% |± 3/2⟩ + 9% |∓ 7/2⟩ + 8% |∓ 3/2⟩ + 5% |± 11/2⟩ + 5% |∓ 5/2⟩	±2.7
274.31	394.73	0.1	0.3	19.0	83.5	34% |± 1/2⟩ + 18% |∓ 3/2⟩ + 15% |± 5/2⟩ + 14% |± 3/2⟩ + 8% |∓ 1/2⟩	±1.5

[a] The angle between the g_z value of the excited Kramers doublet and the ground Kramers doublet.

Table S8. Electronic structure of $[Dy(Cp'')(BH_4)_3]^-$ (where Dy(3) is the central ion) calculated with the crystal field parameters obtained from CASSCF-SO using the solid state geometry of **5-Dy** in zero-field. Each row corresponds to a Kramers doublet.

Energy (cm^{-1})	Energy (K)	g_x	g_y	g_z	Angle[a] (deg)	Wavefunction	$<J_z>$
0.00	0.00	0.1	0.2	19.2	--	91% |± 15/2⟩ + 5% |± 9/2⟩	±7.2
68.78	98.97	0.5	0.8	17.9	44.0	37% |± 11/2⟩ + 26% |± 13/2⟩ + 16% |± 9/2⟩ + 5% |± 15/2⟩ + 5% |∓ 1/2⟩	±5.1
95.35	137.21	2.7	3.8	12.2	40.8	31% |± 7/2⟩ + 26% |± 13/2⟩ + 13% |± 9/2⟩ + 7% |∓ 3/2⟩ + 6% |∓ 5/2⟩ + 5% |∓ 7/2⟩ + 5% |± 5/2⟩	±4.3
143.06	205.86	1.4	4.7	10.2	89.4	19% |± 5/2⟩ + 16% |∓ 5/2⟩ + 15% |± 3/2⟩ + 10% |± 11/2⟩ + 8% |± 13/2⟩ + 7% |∓ 1/2⟩ + 6% |∓ 9/2⟩ + 5% |± 9/2⟩ + 5% |∓ 3/2⟩	±3.2
168.06	241.84	1.8	2.6	13.0	89.2	17% |± 3/2⟩ + 15% |∓ 5/2⟩ + 15% |± 7/2⟩ + 15% |± 1/2⟩ + 10% |∓ 9/2⟩ + 10% |∓ 1/2⟩	±2.5
196.84	283.25	0.3	5.5	11.9	84.1	19% |± 1/2⟩ + 16% |± 3/2⟩ + 13% |± 13/2⟩ + 11% |∓ 7/2⟩ + 8% |∓ 5/2⟩ + 7% |± 9/2⟩ + 7% |± 7/2⟩ + 7% |∓ 1/2⟩ + 6% |∓ 13/2⟩	±3.0
226.41	325.80	1.3	4.1	13.1	60.5	33% |± 11/2⟩ + 21% |± 9/2⟩ + 9% |∓ 7/2⟩ + 7% |± 13/2⟩ + 7% |∓ 5/2⟩+ 6% |∓ 3/2⟩	±4.3
300.09	431.84	0.2	0.6	18.4	85.1	22% |± 3/2⟩ + 21% |∓ 1/2⟩ + 11% |∓ 5/2⟩+ 9% |∓ 11/2⟩ + 8% |∓ 9/2⟩ + 8% |± 7/2⟩ + 6% |± 1/2⟩ + 5% |± 5/2⟩	±2.5

[a] The angle between the g_z value of the excited Kramers doublet and the ground Kramers doublet.

Table S9. Electronic structure of $[Dy(Cp'''')(BH_4)_3]^-$ (where Dy(4) is the central ion) calculated with the crystal field parameters obtained from CASSCF-SO using the solid state geometry of **5-Dy** in zero-field. Each row corresponds to a Kramers doublet.

Energy (cm^{-1})	Energy (K)	g_x	g_y	g_z	Angle[a] (deg)	Wavefunction	$<J_z>$
0.00	0.00	0.0	0.1	19.7	--	97% |± 15/2⟩	±7.4
103.70	149.23	0.5	1.1	17.0	52.3	28% |± 9/2⟩ + 21% |± 11/2⟩ + 15% |± 13/2⟩ + 12% |± 7/2⟩ + 6% |∓ 5/2⟩	±4.6
137.49	197.85	2.9	6.5	11.3	72.2	26% |± 7/2⟩ + 22% |± 5/2⟩ + 15% |∓ 7/2⟩ + 8% |∓ 13/2⟩ + 7% |∓ 11/2⟩ + 6% |∓ 9/2⟩ + 5% |∓ 5/2⟩	±3.6
174.28	250.79	1.5	4.1	8.5	54.9	18% |± 3/2⟩ + 14% |∓ 13/2⟩ + 12% |∓ 9/2⟩ + 12% |± 5/2⟩ + 9% |± 9/2⟩ + 7% |∓ 3/2⟩ + 6% |± 7/2⟩ + 5% |∓ 7/2⟩	±3.4
203.70	293.13	0.1	1.0	9.2	44.6	14% |± 13/2⟩ + 13% |∓ 13/2⟩ + 12% |∓ 9/2⟩ + 10% |± 7/2⟩ + 10% |∓ 5/2⟩ + 6% |∓ 7/2⟩ + 6% |± 1/2⟩ + 6% |∓ 1/2⟩ + 5% |∓ 11/2⟩ + 5% |± 5/2⟩ + 5% |∓ 3/2⟩	±4.0
223.85	322.12	0.4	4.4	11.1	47.5	35% |± 11/2⟩ + 15% |± 13/2⟩ + 12% |± 1/2⟩ + 9% |± 9/2⟩ + 7% |∓ 1/2⟩ + 5% |∓ 13/2⟩ + 5% |∓ 9/2⟩ + 5% |± 3/2⟩	±4.2
254.27	365.90	0.6	4.2	10.2	86.3	19% |± 3/2⟩ + 13% |± 5/2⟩ + 13% |∓ 5/2⟩ + 13% |± 1/2⟩ + 9% |∓ 3/2⟩ + 8% |∓ 7/2⟩ + 6% |∓ 11/2⟩ + 5% |± 11/2⟩	±2.7
286.71	412.58	1.0	4.4	14.4	84.2	36% |± 1/2⟩ + 16% |± 3/2⟩ + 10% |∓ 11/2⟩ + 10% |∓ 1/2⟩ + 7% |∓ 9/2⟩ + 7% |∓ 3/2⟩	±2.0

[a] The angle between the g_z value of the excited Kramers doublet and the ground Kramers doublet.

7. References

[1] B. Wrackmeyer, *Ann. Rep. NMR Spectrosc*. **1988**, *20*, 61.

[2] *CrysAlisPRO ver.* 39.27b, **2017** (Oxford Diffraction /Agilent Technologies UK Ltd: Yarnton, England).

[3] G. M. Sheldrick, *Acta Crystallogr*. **2008**, *A64*, 112.

[4] G. M. Sheldrick, *Acta Crystallogr.* **2015**, *C71*, 3.

[5] O. V. Dolomanov, L. J. Bourhis, R. J. Gildea, J. A. K. Howard, H. Puschmann, *J. Appl. Crystallogr*. **2009**, *42*, 339.

[6] L. J. Farrugia, *J. Appl. Crystallogr.* **2012**, *45*, 849.

[7] *POV-Ray*, *ver. 3.7.0*, **2013** (Persistence of Vision Raytracer Pty. Ltd, Williamstown, VIC).

[8] I. Fdez. Galván, M. Vacher, A. Alavi, C. Angeli, F. Aquilante, J. Autschbach, J. J. Bao, S. I. Bokarev, N. A. Bogdanov, R. K. Carlson, L. F. Chibotaru, J. Creutzberg, N. Dattani, M. G. Delcey, S. S. Dong, A. Dreuw, L. Freitag, L. M. Frutos, L. Gagliardi, F. Gendron, A. Giussani, L. González, G. Grell, M. Guo, C. E. Hoyer, M. Johansson, S. Keller, S. Knecht, G. Kovačević, E. Källman, G. Li Manni, M. Lundberg, Y. Ma, S. Mai, J. P. Malhado, P. Å. Malmqvist, P. Marquetand, S. A. Mewes, J. Norell, M. Olivucci, M. Oppel, Q. M. Phung, K. Pierloot, F. Plasser, M. Reiher, A. M. Sand, I. Schapiro, P. Sharma, C. J. Stein, L. K. Sørensen, D. G. Truhlar, M. Ugandi, L. Ungur, A. Valentini, S. Vancoillie, V. Veryazov, O. Weser, T. A. Wesołowski, P.-O. Widmark, S. Wouters, A. Zech, J. P. Zobel, R. Lindh, *J. Chem. Theory Comput.* **2019**, *15*, 5925.

[9] B. O. Roos, R. Lindh, P. Å. Malmqvist, V. Veryazov, P. O. Widmark, *J. Phys. Chem. A* **2004**, *108*, 2851.

[10] B. O. Roos, R. Lindh, P. Å. Malmqvist, V. Veryazov, P. O. Widmark, *J. Phys. Chem. A* **2005**, *109*, 6575.

[11] L. Ungur, L. F. Chibotaru, *Chem. Eur. J.* **2017**, *23*, 3708.

[12] *Diamond - Crystal and Molecular Structure Visualization*, *ver. 4.6.6* (Eds H. Putz, K. Brandenburg) **2021** (Crystal Impact GbR, Bonn).